Thermoflow Multiplicity in a Packed-Bed Reactor

Part I: Adiabatic Case

Steady states with different flow rates and temperature profiles may exist in a packed-bed reactor operating under a prescribed pressure drop, due to the coupling among the species, energy, and momentum balances and the change of the physical properties with temperature and pressure. This *thermoflow multiplicity* may be found even for reactions whose rate is rather insensitive to temperature changes (low activation energy) and may lead to highly undesirable operation of multitube packed-bed reactors. A hierarchy of models based on different assumptions is used to derive criteria for predicting the conditions under which this thermoflow multiplicity may occur.

J. P. Lee, V. Balakotaiah and Dan Luss
Department of Chemical Engineering
University of Houston
Houston, TX 77004

Introduction

Many theoretical and experimental studies of steady state multiplicities of packed-bed reactors have been reported in the literature. Some recent experimental findings have been reported by Hegedus et al. (1977), Hlavacek and Votruba (1978), Sharma and Hughes (1979), Paspek and Varma (1980), and Wedel and Luss (1984). Most previous theoretical studies were of multiplicity caused by the interaction among the chemical and the heat and mass transport rate processes. These studies ignored the momentum transport in the reactor and assumed that the qualitative multiplicity features are not affected by the interaction among the momentum transport, the chemical reaction, and the change in the physical properties of the fluid with temperature.

Several studies revealed that in a variety of systems steady states with different flow rates may exist under the same pressure drop. This behavior, which we define as *thermoflow multiplicity,* is caused by the interaction among the species, energy, and momentum balances and the sensitive dependence of the physical properties on the state variables (temperature, pressure, composition). For example, different flow rates may exist under the same pressure drop for simple flows of nonreactive fluids, the viscosity of which is highly temperature-sensitive (Pearson et al., 1973; Merzhanov and Stolin, 1974; Davis et al., 1983; Pearson, 1985). Moreover, two different stable states with different heat loads may exist in an evaporator tube operating under a fixed pressure drop (Ledinegg, 1938; Dogan et al., 1983). Gupalo and Ryazantsev (1968) showed that thermoflow multiplicity can occur in a tubular reactor when the flow is laminar and the fluid is incompressible. Goldshtik (1979) found a similar behavior when an incompressible fluid flows through a granular bed in which heat is produced uniformly. Bostandzhiyan et al. (1979), Zhirkov et al. (1980), and Vaganov and Zhirkov (1986) found thermoflow multiplicity in a tubular polymerization reactor in which viscosity was strongly dependent on the temperature and degree of polymerization. Matros and Chumakova (1980) showed an example of thermoflow multiplicity in a packed-bed reactor in which the reactant was incompressible.

Multitube packed-bed reactors are used in many industrial processes. In these reactors the total pressure drop is the same for all the tubes, and the flow rate in each tube depends on the pressure drop, the packed catalyst, and the profile of the physical properties of the fluid, such as density and viscosity. The temperature profile in all the tubes should be essentially the same in order to avoid undesirable mechanical stresses that can damage the reactor. This profile depends on the rate of heat release by the chemical reaction, which depends in turn on the flow rate. When an exothermic gaseous reaction is carried out in a tube, a small increase in the feed velocity reduces the temperature at all points within the reactor. This increases the local density and requires an additional increase in the feed mass flow rate to maintain the prescribed pressure drop. This positive feedback mechanism can lead to thermoflow multiplicity. A natural

Correspondence concerning this paper should be addressed to V. Balakotaiah and Dan Luss.

question is what is the set of conditions (parameter values) under which states with different flow rates and temperature profiles may exist in adjacent tubes.

The goal of this study is to gain an understanding of the factors that may lead to thermoflow multiplicity in an adiabatic packed-bed reactor operating under a specified pressure drop, and to derive criteria predicting the conditions (parameters) under which it occurs. This work is the first step in this study and describes the reactor by a pseudohomogeneous one-dimensional model with no axial dispersion. This model has a unique steady state solution if the inlet velocity is specified. Thus, the multiplicity is due to the fact that when the physical properties of the fluid depend on the temperature and conversion, different inlet velocities may exist under the same pressure drop.

In this study we divide the global parameter space of the governing mathematical model into regions with different types of bifurcation diagrams. This information is used to focus attention on the key factors that may lead to thermoflow multiplicity and the conditions under which it may occur.

Development of Mathematical Model

Consider an adiabatic packed-bed reactor in which a single, exothermic, irreversible chemical reaction $A \rightarrow B$ occurs. We assume that the total pressure drop across the bed is specified and determines the flow rate. We describe the reactor by a pseudohomogeneous one-dimensional plug-flow model that ignores any axial dispersion of either species or energy. The corresponding steady state continuity, species, energy, and momentum balances are

$$\frac{d}{d\ell}(\rho u) = 0 \tag{1}$$

$$\frac{d}{d\ell}(uC) = -r \tag{2}$$

$$\rho u c_p \frac{dT}{d\ell} = (-\Delta H) r \tag{3}$$

$$\frac{dP}{d\ell} + \rho u \frac{du}{d\ell} = -f_p \tag{4}$$

where the local frictional pressure drop is computed from the Ergun equation

$$f_p = A\mu u + B(\rho u)u \tag{5}$$

where A and B are constants that depend on the properties of the packing. The corresponding boundary conditions are:

$$P = P_o, \quad C = C_o, \quad T = T_o \quad \text{at } \ell = 0 \tag{6}$$

$$P = P_{exit} \quad \text{at } \ell = L\ . \tag{7}$$

When the density and the viscosity of the fluid are independent of temperature, pressure, and conversion, the momentum balance, Eq. 4, is decoupled from the species and energy balances and the velocity is determined uniquely by the momentum balance and continuity equation. The corresponding unique set of concentration and temperature profiles are determined uniquely by Eqs. 2 and 3. This indicates that the commonly neglected change in physical properties is essential for the occurrence of steady state multiplicity in this model.

We assume that the fluid in the bed is a gas the density of which satisfies the ideal gas law

$$\rho = \frac{PM_w}{RT} \tag{8}$$

and that its viscosity is independent of conversion and pressure and increases with temperature according to the relation

$$\mu = \mu(T_o)\left(\frac{T}{T_o}\right)^{\delta} \tag{9}$$

where δ is a positive constant, usually between 0.5 and 1. Integration of Eq. 1 gives

$$\rho u = \rho_o u_o. \tag{10}$$

Substitution of the ideal gas law into the continuity equation, Eq. 10, gives

$$u = u_o \frac{TP_o}{T_o P}. \tag{11}$$

Differentiation of Eq. 11 with respect to ℓ gives

$$\frac{du}{d\ell} = \frac{u_o P_o}{P}\left(\frac{1}{T_o}\frac{dT}{d\ell} - \frac{T}{T_o P}\frac{dP}{d\ell}\right). \tag{12}$$

Subsitution of Eq. 12 into Eq. 4 and use of Eqs. 5 and 10 gives

$$\left[1 - \frac{\rho_o u_o^2}{P_o}\frac{T}{T_o}\left(\frac{P_o}{P}\right)^2\right]\frac{dP}{d\ell} + \frac{\rho_o u_o^2}{T_o}\left(\frac{P_o}{P}\right)\frac{dT}{d\ell} = -(A\mu u + B\rho u^2). \tag{13}$$

Under practical conditions $\rho_o u_o^2$ is significantly smaller than P_o (the ratio is usually smaller than 10^{-5}) so that the second term in the parenthesis multiplying $dP/d\ell$ in Eq. 13 is very small compared to unity. We omitted this term to simplify the analysis significantly. The impact of this approximation is discussed in a later section.

Multiplying Eq. 2 by $-\Delta H$, adding it to Eq. 3, and integrating gives

$$\frac{T}{T_o} = 1 + \frac{(-\Delta H)C_o}{\rho_o c_p T_o}\left(\frac{u_o C_o - uC}{u_o C_o}\right) \tag{14}$$

which can be rewritten as

$$y = 1 + \beta x \tag{15}$$

where the conversion

$$x = \frac{u_o C_o - uC}{u_o C_o} \tag{16}$$

and

$$y = \frac{T}{T_o} \qquad \beta = \frac{(-\Delta H)C_o}{\rho_o c_p T_o} \tag{17}$$

To simplify the algebraic manipulations required to determine the structure of the solutions, we assume that the reaction is of zero order, i.e.,

$$r(C, T) = k(T)H(C) = k(T_o)X(y)H(C) \tag{18}$$

where $H(C)$ is the Heaviside function and

$$X(y) = k(T)/k(T_o) = \exp\left[\frac{E}{RT_o}\left(1 - \frac{1}{y}\right)\right]. \tag{19}$$

Introducing the dimensionless variables

$$\Pi = \frac{P}{P_o} \qquad z = \frac{\ell}{L}$$

$$\gamma = \frac{E}{RT_o} \qquad Da = \frac{k(T_o)L}{u_o C_o}$$

$$E_1 = \frac{A\mu(T_o)k(T_o)L^2}{P_o C_o} \qquad E_2 = \frac{B\rho_o k(T_o)^2 L^3}{P_o C_o^2}$$

$$E_3 = \frac{\rho_o k(T_o)^2 L^2}{P_o C_o^2} \tag{20}$$

the energy and momentum balances can be written as

$$\frac{dy}{dz} = \beta Da X(y) H(1 + \beta - y) \tag{21}$$

$$\frac{1}{2}\frac{d\Pi^2}{dz} = -\frac{E_1 y^{1+\delta}}{Da} - \frac{E_2 y}{Da^2} - \frac{E_3}{Da^2}\frac{dy}{dz} \tag{22}$$

subject to the conditions

$$y(0) = \Pi(0) = 1, \qquad \Pi(1) = \Pi_1. \tag{23}$$

Equations 21–23 can be solved for any Da and the parameter vector

$$p^T = (\gamma, \beta, \delta, E_1, E_2, E_3). \tag{24}$$

For a specified p a solution of Eqs. 21–23 exists only for one or a few values of Da, which is proportional to $1/u_o$. In other words, there exist at most several inlet velocities for which it is possible to operate under the prescribed pressure drop.

The steady state equation, which describes the dependence of Da, or equivalently the inlet velocity, on the exit pressure Π_1, may be obtained by integrating Eqs. 21 and 22. Due to the discontinuous nature of the reaction rate, we consider separately those cases for which incomplete conversion occurs, i.e., $y_1 < 1 + \beta$, and those with complete conversion, i.e., $y_1 = 1 + \beta$.

When the conversion is not complete ($y_1 < 1 + \beta$), integration of Eq. 21 gives

$$G(y_1, Da, p) = \beta Da - J(y_1, 0) = 0 \tag{25}$$

where we define

$$J(y_1, \alpha) = \int_1^{y_1} y^\alpha X^{-1}(y)\, dy. \tag{26}$$

Dividing Eq. 22 by Eq. 21 and integrating gives

$$F_1(Da, \Pi_1, p) = 1 - \Pi_1^2 - \frac{2E_1}{\beta Da^2} J(y_1, 1 + \delta) - \frac{2E_2}{\beta Da^3} J(y_1, 1) - \frac{2E_3(y_1 - 1)}{Da^2} = 0 \tag{27}$$

In solving Eq. 27 one needs to use Eq. 25 to determine the monotonic dependence of y_1 on Da for the specific p.

We define Da^* to be the smallest value of Da (largest u_o) for which the conversion is complete, i.e., $y_1 = 1 + \beta$. It can be computed by the expression

$$\beta Da^* = J(1 + \beta, 0) \tag{28}$$

When $Da > Da^*$ (i.e., $u_o < u_o^*$) the reactant is completely consumed at $z_c = Da^*/Da$ and $y_1 = 1 + \beta$ for $z_c < z < 1$. Dividing Eq. 22 by Eq. 21 and integrating gives

$$1 - \Pi_c^2 - \frac{2E_1 J(1 + \beta, 1 + \delta)}{\beta Da^2} - \frac{2E_2 J(1 + \beta, 1)}{\beta Da^3} - \frac{2E_3\beta}{Da^2} = 0 \tag{29}$$

where Π_c is the dimensionless pressure at z_c. Integrating Eq. 22 from z_c to $z = 1$ and combining with Eq. 29 gives

$$F_2(Da, \Pi_1, p) = 1 - \Pi_1^2 - \frac{2E_1 J(1 + \beta, 1 + \delta)}{\beta Da^2} - \frac{2E_2 J(1 + \beta, 1)}{\beta Da^3} - \left[\frac{2E_1(1 + \beta)^{1+\delta}}{Da} + \frac{2E_2(1 + \beta)}{Da^2}\right] \cdot \left[1 - \frac{J(1 + \beta, 0)}{\beta Da}\right] - \frac{2E_3\beta}{Da^2} = 0. \tag{30}$$

Thus, the steady state equation takes the form

$$F(Da, \Pi_1, p) \equiv \begin{cases} F_1 = 0, & Da < Da^* \\ F_2 = 0, & Da > Da^* \end{cases} \tag{31}$$

where F_1 and F_2 are defined by Eqs. 27 and 30, respectively.

We note that the function defined by Eq. 31 has the following properties:

1. F is continuous for all $Da > 0$.
2. $F(Da = 0) = -\infty$ and $F(Da = \infty) = 1 - \Pi_1^2$. This indicates that at least one steady state solution exists for any $0 < \Pi_1 < 1$ and that the number of solutions is odd.
3. The first derivative of F with respect to Da is not continuous at $Da = Da^*$ unless $E_3 = 0$.

4. The second and higher derivatives are not continuous at $Da = Da^*$.

Mathematical Background

We wish to determine the set of conditions (parameter values) for which several values of Da (inlet velocities) satisfy steady state Eq. 31 for the same pressure drop. To accomplish this we follow the scheme of Balakotaiah and Luss (1981) and construct hypersurfaces, which divide the global parameter space into regions having qualitatively different types of bifurcation diagrams of Da vs. Π_1. Before constructing these surfaces we reduce the number of parameters in the model by one by defining

$$\Lambda_j = \frac{E_j}{1 - \Pi_1^2} \qquad j = 1, 2, 3 \tag{32}$$

so that steady state Eqs. 27 and 30 become

$$F_1(Da, \Lambda_j, \boldsymbol{p}) = \frac{1}{\Lambda_j} - \frac{2J(y_1, 1 + \delta)E_1/E_j}{\beta Da^2} - \frac{2J(y_1, 1)E_2/E_j}{\beta Da^3} - \frac{2(y_1 - 1)E_3/E_j}{Da^2} = 0 \tag{33}$$

$$F_2(Da, \Lambda_j, \boldsymbol{p}) = \frac{1}{\Lambda_j} - \frac{2J(1 + \beta, 1 + \delta)E_1/E_j}{\beta Da^2} - \frac{2J(1 + \beta, 1)E_2/E_j}{\beta Da^3} - \left(\frac{2(1 + \beta)^{1+\delta}E_1/E_j}{Da} + \frac{2(1 + \beta)E_2/E_j}{Da^2}\right)\left(1 - \frac{J(1 + \beta, 0)}{\beta Da}\right) - \frac{2\beta E_3/E_j}{Da^2} = 0. \tag{34}$$

Note that the vector $\boldsymbol{p}$ consists only of five parameters, namely, γ, β, δ and two E_i/E_j where $i \neq j$.

A hysteresis loop in the bifurcation diagram of Da vs. Λ_j emerges or collapses (an ignition and an extinction point coalesce) upon crossing the *hysteresis variety* (H), which is the set of parameters $\boldsymbol{p}$ at which

$$F_i = 0 \tag{35a}$$

$$\frac{dF_i}{dDa} = 0 \tag{35b}$$

$$\frac{d^2F_i}{dDa^2} = 0 \tag{35c}$$

for $i = 1$ or 2. By eliminating Da and Λ_j from Eqs. 35a–c we obtain the hysteresis variety in the five-dimensional parameter space $\boldsymbol{p}$. Computationally it is convenient to construct the variety by finding first the set H^* of the parameters $\boldsymbol{p}$ satisfying Eqs. 35b and 35c (note that Λ_j does not appear in these two equations and to construct H^* we only need to eliminate Da). Clearly, H is the subset of points on H^* for which Eq. 35a is satisfied for some feasible Λ_j.

It can be shown (Lee, 1987) that Eqs. 35 cannot be satisfied when $i = 2$. This implies that a hysteresis loop cannot emerge or disappear on the branch of states with complete conversion, i.e., $Da > Da^*$. However, a hysteresis loop can emerge or disappear at $Da = Da^*$ due to the discontinuous derivatives of the steady state Eq. 31. We define in these situations a *generalized hysteresis variety* (GH) to be the set of parameters for which

$$F_1(Da^*) = 0 \tag{36a}$$

$$\frac{dF_1}{dDa}(Da^*) = 0 \tag{36b}$$

and

$$F(Da^* - \epsilon)F(Da^* + \epsilon) < 0. \tag{36c}$$

where ϵ is an arbitrarily small positive number.

Computationally, it is convenient to find first the set g^* of parameters $\boldsymbol{p}$ satisfying Eqs. 36b and 36c. Clearly, the generalized hysteresis variety is the subset of points on g^* that satisfy Eq. 36a for some feasible Λ_j.

Cases *a* and *b* in Figure 1 illustrate the qualitative changes that occur in the bifurcation diagram when the parameters cross the hysteresis or generalized hysteresis variety.

When steady state Eq. 31 has more than three solutions for some Π_1, the qualitative features of the bifurcation diagram change when the relative positions of various limit (ignition and extinction) points change. This occurs when the parameters cross the *double limit variety*, which is defined by the four equations

$$F(Da_1) = \frac{dF}{dDa}(Da_1) = 0 \tag{37a}$$

$$F(Da_2) = \frac{dF}{dDa}(Da_2) = 0; \quad Da_1 \neq Da_2. \tag{37b}$$

Elimination of Da_1, Da_2, and Λ_j from Eqs. 37a and 37b gives the double limit variety in the parameter space. When the first derivative is not continuous, we define the *generalized double*

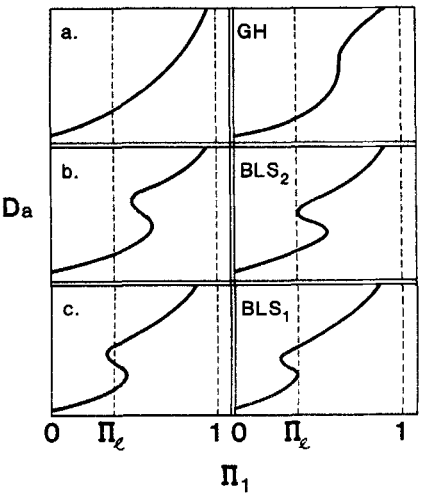

Figure 1. Typical *Da* vs. Π_1 bifurcation diagrams and those corresponding to parameters on GH, BLS_1, and BLS_2.

limit variety by Eq. 37a and

$$F(Da^*) = 0 \tag{37c}$$

$$F(Da^* - \epsilon)F(Da^* + \epsilon) > 0; \quad Da^* \neq Da_1 \tag{37d}$$

The qualitative features of a bifurcation diagram of Da vs. Λ_j change also when the parameters cross the *isola variety*, which is defined by Eqs. 35a, 35b, and

$$\frac{\partial F_i}{\partial \Lambda_j}(Da, \Lambda_j, \boldsymbol{p}) = 0, \tag{38}$$

where $i = 1$ or 2. This variety cannot exist in the present problem as Eq. 38 is never satisfied.

In practice, the dimensionless exit pressure Π_1 must exceed some limiting value which we denote by Π_ℓ. We consider the multiplicity features that are within the feasible region $\Pi_\ell < \Pi_1 < 1$.

The qualitative features of the bifurcation diagram of Da vs. Λ_j change also upon crossing the *boundary limit set* (BLS), which is the set of parameters for which a limit point exists for the limiting feasible exit pressure Π_ℓ, that is, Eqs. 35a and 35b are satisfied for $\Pi_1 = \Pi_\ell$ (Balakotaiah and Luss, 1984). We define by BLS_1 (BLS_2) the set of parameters for which an ignition (extinction) point exists at $\Pi_1 = \Pi_\ell$. The transitions occurring at the BLS_1 and BLS_2 are shown in Figure 1. We conclude that a change in the features of the bifurcation diagram of Eq. 31 requires crossing of either the hysteresis variety (H or GH), BLS_1, BLS_2, or the double limit variety.

Analysis of Limiting Cases

The parameter vector $\boldsymbol{p}$ contains five parameters and this complicates the analysis and the construction and presentation of the various boundaries. To simplify this task we start by studying separately three limiting cases in which only one of the three $E_i (i = 1, 2, 3)$ is different from zero, i.e., only one term (mechanism) contributes to the pressure drop in Eq. 22. We then consider the more general case in which one of the three E_i vanishes, i.e., we account for two types of pressure loss mechanisms. Finally, in the following section we examine the general case in which all three E_i have positive values. This approach enables us to find the impact of each pressure loss mechanism on the multiplicity features.

Limiting case a, laminar pressure loss

The limiting case in which $E_2 = E_3 = 0$ corresponds to situations in which the second term in the Ergun equation is negligible in comparison to the first and the momentum change due to the thermal expansion of the fluid is negligible in comparison to the laminar frictional pressure loss.

Steady state Eqs. 33 and 34 simplify in this case to

$$F_1 = \frac{1}{\Lambda_1 \beta} - \frac{2J(y_1, 1 + \delta)}{(\beta Da)^2} = 0 \tag{39a}$$

where y_1 satisfies Eq. 25 and

$$F_2 = \frac{1}{\Lambda_1 \beta} - \frac{2J(1 + \beta, 1 + \delta)}{(\beta Da)^2} - \frac{2(1 + \beta)^{1+\delta}}{\beta Da} \cdot \left[1 - \frac{J(1 + \beta, 0)}{\beta Da}\right] = 0. \tag{39b}$$

It can be shown that there exists no Da value for which the three Eqs. 35 are satisfied, i.e., no hysteresis variety exists. Differentiation of F indicates that both F and dF/dDa are continuous for all Da but that d^2F/dDa^2 is discontinuous at Da^*, suggesting that a generalized hysteresis variety exists. To find it we use Eq. 25 to rewrite $dF_1/dDa = 0$ as

$$g_1(\gamma, y_1) = 2J(y_1, 1 + \delta) - y_1^{1+\delta} J(y_1, 0) = 0. \tag{40}$$

The equation $g_1(\gamma, 1 + \beta) = 0$ defines a set of (γ, β) values that satisfy Eq. 36b. It can be proven (Lee, 1987) that these points satisfy also the condition of Eq. 36c and therefore define a g_1^* set. The graph of g_1^* is shown as a solid line AB in Figure 2 for $\delta = 0.5$. It approaches asymptotically for $\gamma \to \infty$ the line

$$\beta = 2^{1/(1+\delta)} - 1 \ (= 0.587 \text{ for } \delta = 0.5) \tag{41}$$

and intersects the $\gamma = 0$ axis at a β value given by the equation

$$\Gamma \equiv (1 + \beta)^{1+\delta}(2 - \delta\beta) - 2 = 0. \tag{42}$$

Solution of Eq. 42 gives $\beta = 3.594$ for $\delta = 0.5$. We note that γ is a monotonic decreasing function of β along the g_1^* curve shown in Figure 2. We conclude that for a gaseous mixture thermoflow multiplicity can occur only for an exothermic reaction when the viscosity increases with increasing temperature.

The value of Λ_1 corresponding to each hysteresis point on g_1^* may be found by solving Eq. 36a for specific (γ, β) values. Numerical calculations for $\delta = 0.5$ show that the value of Λ_1 along the g_1^* curve increases from 0.1016 at $\gamma = 0$, $\beta = 3.594$ (point A) to 0.1032 at $\gamma \equiv \gamma^* = 0.76$ and $\beta \equiv \beta^* = 2.55$. For β values to the left of β^*, Λ_1 decreases monotonically from 0.1032 to zero. Thus, the value of Λ_1 at a hysteresis point must be positive and smaller than 0.1032. We conclude that a monotonic Da vs. Λ_1 bifurcation diagram (case *a* in Figure 1) is obtained if

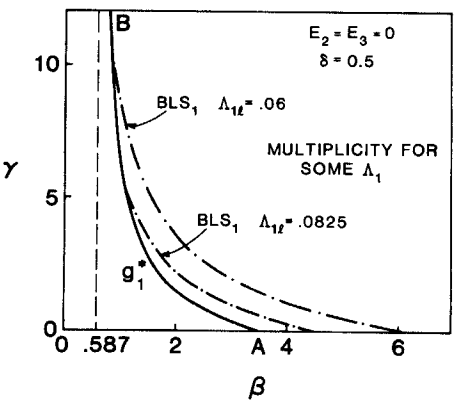

Figure 2. Dependence of uniqueness boundaries g_1^* and BLS_1 on γ, β, and $\Lambda_{1\ell}$ for limiting case *a* (laminar pressure loss).

$$\Lambda_{1\ell} = \frac{E_1}{1 - \Pi_\ell^2} > 0.1032. \tag{43}$$

Clearly, the condition in Eq. 43 is a sufficient uniqueness criterion. Thus, thermoflow multiplicity is more likely to occur in reactors with a large pressure drop, i.e., small $\Lambda_{1\ell}$.

The generalized hysteresis variety (GH) is the locus of points on the g_1^* curve for which a hysteresis point exists for a Λ_1 value larger than $\Lambda_{1\ell}$. At each point on the GH variety two limit points (ignition and extinction) coalesce. The coalescence of the two limit points at $Da = Da^*$ and $y_1 = 1 + \beta$ implies that at any ignition point $Da < Da^*$ and $y_1 < 1 + \beta$, i.e., the reactant is not completely consumed. On the other hand, at any extinction point $Da > Da^*$ and $y_1 = 1 + \beta$, so that the reactant is completely converted for all the states on the ignited branch.

Da is a single-valued function of Λ_1, or equivalently Π_1, for any (γ, β) to the left of the g_1^* graph. Thus, a sufficient condition for uniqueness is that

$$\beta < 2^{1/(1+\delta)} - 1 \; (= 0.587 \text{ for } \delta = 0.5). \tag{44}$$

An analytical derivation of this sufficient condition can be obtained by noting that $J(y_1, 1 + \delta) > J(y_1, 0)$ for all $y_1 > 1$. Thus, Eq. 40 implies that g_1 cannot vanish if $2 > y_1^{1+\delta}$. Thus, a GH cannot exist if $2 > (1 + \beta)^{1+\delta}$, or equivalently if Eq. 44 is satisfied.

Steady state multiplicity is observed only if the Da vs. Π_1 bifurcation diagram has two limit points [i.e., for (γ, β) values to the right of g_1^*] and the outlet pressure for the ignition point exceeds Π_ℓ (cases b and c in Figure 1). When the outlet pressure of the ignition point is equal to Π_ℓ, a transition from uniqueness to multiplicity occurs as the parameters are perturbed. The BLS_1 (Figure 1) is the set of parameters for which an ignition point exists at Π_ℓ. To find it, we combine steady state Eq. 39a with Eq. 25 to get

$$\frac{1}{\beta\Lambda_{1\ell}} = \frac{2J(y_1, 1 + \delta)}{J^2(y_1, 0)} \tag{45}$$

For any specified $\Lambda_{1\ell}$, the BLS_1 is found by a simultaneous solution of Eqs. 45 and 40 using y_1 as a parameter. A simultaneous solution of these equations for $\delta = 0.5$ gives the curve shown in Figure 3. Multiple solutions can exist (ignition point is in the feasible region) only for parameters to the left of this curve. It is possible to check if multiplicity exists for some β, γ and $\Lambda_{1\ell}$ by inspection of Figures 2 and 3. Figure 3 shows that a unique solution exists for all $\Lambda_1 > \Lambda_{1\ell}$ if

$$\beta > \frac{0.365}{\Lambda_{1\ell}} = \frac{0.365\,(1 - \Pi_\ell^2)}{E_1} \tag{46}$$

We define a multiplicity region to be the (γ, β) values bounded by the GH and BLS_1, and for which three Da values satisfy the steady state equation for some $\Lambda_1 \geq \Lambda_{1\ell}$, or equivalently for some $\Pi_1 \geq \Pi_\ell$. For $\Lambda_{1\ell}$ in (0.1016, 0.1032) the BLS_1 intersects the GH at two points, one to the left of (γ^*, β^*) and one to the right of it. In this case the multiplicity region has the shape of a narrow crescent. For $\Lambda_{1\ell} < 0.1016$ the BLS_1 intersects

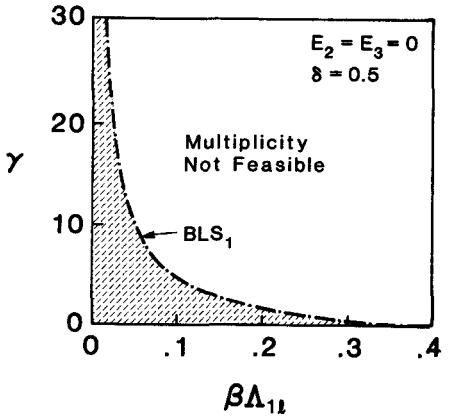

Figure 3. Dependence of uniqueness boundary BLS_1 on γ and $\beta\Lambda_{1\ell}$ for limiting case *a* (laminar pressure loss).

the GH only at one point and the multiplicity region has the shape of a wedge, Figure 2.

Boundary limit set 2 (BLS_2) is the boundary of the parameters at which the extinction point shifts from within (Figure 1, case b) to outside the feasible region (Figure 1, case c). The BLS_2 can be found by a simultaneous solution of Eq. 39b and $dF_2/dDa = 0$ for the specified $\Lambda_{1\ell}$.

The GH, BLS_1, and BLS_2 divide the (γ, β) plane into three regions. In one region, denoted as a in Figure 4, Da is a monotonic function of Λ_1 or Π_1 so that a unique Da, or equivalently inlet velocity, exists for any exit pressure. In the other two regions, b and c in Figure 4, three Da values exist for some $\Pi_1 > \Pi_\ell$.

The multiplicity region for sufficiently small $\Lambda_{1\ell}$ (<0.1016) has a wedge shape in the (γ, β) plane. Thus, thermoflow multiplicity can occur even if $\gamma = 0$, i.e., the reaction rate constant is insensitive to temperature changes. This multiplicity is due to the change of physical properties of the fluid with temperature, the specified pressure drop, and the dependence of the heat release on the residence time. This feedback is rather different from the thermokinetic feedback mechanism that is the cause of multiplicity in the traditional models of packed-bed reactors, which do not account for the momentum balance.

All three sufficient uniqueness criteria, Eqs. 43, 44, and 46,

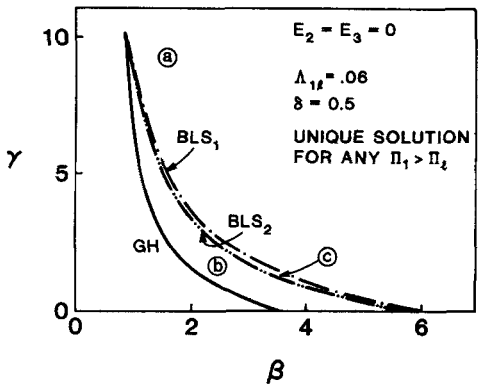

Figure 4. Division of (γ, β) plane into regions with different Da vs. Π_1 bifurcation diagrams.
Letters refer to diagrams shown in Figure 1.

have to be violated for multiplicity to occur for some Λ_1. Of these three criteria, Eq. 46 is usually not a limiting one as multiplicity exists only if $\Lambda_{1g} < 0.1032$ (the condition in Eq. 43). In such cases the condition in Eq. 46 is not satisfied for any $\beta < 3.5$, which is true for most exothermic reactions.

The impact of the temperature dependence of the viscosity on the multiplicity region can be seen from Eqs. 41 and 42. When the viscosity does not depend on the temperature ($\delta = 0$), the g_1^* curve does not intersect the β axis and the vertical asymptote in Figure 2 (point B) is at $\beta = 1$, i.e., multiplicity exists provided $\beta > 1$. On the other hand, for a linear temperature dependence of the viscosity ($\delta = 1$), the g_1^* curve intersects the β axis at $\beta = 1.732$ and the vertical asymptote is at $\beta = 0.414$. Thus, the multiplicity region is enlarged with increasing δ values. These facts point out that *for exothermic gaseous reactions the main cause of the thermoflow multiplicity is the change of density with temperature* and that the change of viscosity with temperature only enhances that feedback.

The cause of the thermoflow multiplicity may be understood better by inspection of Figure 5, which shows the dimensionless pressure, temperature, and velocity profiles in the bed [the velocity was normalized by $k(T_o)L/C_o$). One solution (case *1*) corresponds to a rather high inlet velocity for which the conversion is low. Thus, the temperature is almost constant and the pressure is almost a linear function of position. The other two solutions (cases *2* and *3*) are for lower inlet velocities. In these cases a high conversion occurs leading to a rapid temperature increase and a corresponding density decrease. While the upstream pressure drop for these cases is lower than that of case *1*, the inverse is true at the downstream and the same overall pressure drop exists for all three cases.

Limiting case b, turbulent pressure loss

The limiting case $E_3 = E_1 = 0$ corresponds to situations in which the value of the laminar pressure drop in the Ergun equation is very small compared to that of the turbulent pressure drop, i.e., $A\mu \ll B\rho_o u_o$ and the momentum change due to the thermal expansion of the gas is negligible in comparison to the frictional pressure loss. Steady state Eqs. 33 and 34 simplify in this case to

$$F_1(Da, \Lambda_2, p) = \frac{1}{\Lambda_2 \beta^2} - \frac{2J(y_1, 1)}{(Da\beta)^3} = 0 \qquad (47)$$

where y_1 satisfies Eq. 25 and

$$F_2(Da, \Lambda_2, p) = \frac{1}{\Lambda_2 \beta^2} - \frac{2J(1+\beta, 1)}{(Da\beta)^3} - \frac{2(1+\beta)}{(Da\beta)^2}\left[1 - \frac{J(1+\beta, 0)}{Da\beta}\right] = 0. \qquad (48)$$

The analysis of this case is rather similar to that of case *a*. It can be shown that a hysteresis variety cannot exist for any $Da > Da^*$, i.e., no parameters exist for which Eqs. 35a–c are satisfied for F_2. However, a hysteresis variety can exist for $Da < Da^*$ since Eqs. 35b and 35c have for all $\beta \geq 15.22$ the solution

$$\gamma = 3.65 \quad y_1 = 16.22. \qquad (49)$$

This H^* set is shown by the solid line segment GA in Figure 6.

To find the generalized hysteresis variety we use Eq. 25 to express $dF_1/dDa = 0$ as

$$g_2(\gamma, y_1) \triangleq 3J(y_1, 1) - y_1 J(y_1, 0) = 0. \qquad (50)$$

The equation

$$g_2(\gamma, 1+\beta) = \int_1^{1+\beta} [3y - (1+\beta)]X^{-1}(y)\, dy = 0 \qquad (51)$$

has no solution for $\beta < 2$ since the integrand is positive. A unique positive value of γ satisfies Eq. 51 for any $\beta > 2$. All the solutions for $\beta < 15.22$ (shown as solid line segment GB in Figure 6) satisfy the conditions of Eq. 36c and belong therefore to the g_2^*

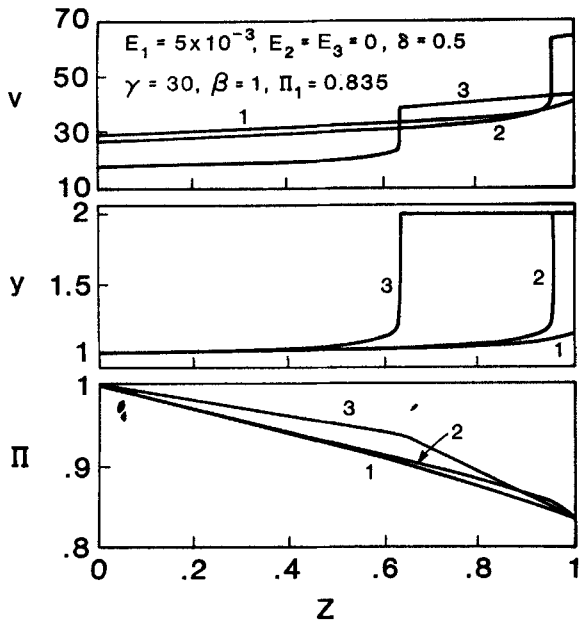

Figure 5. Dimensionless velocity, temperature, and pressure profiles corresponding to the same pressure drop.

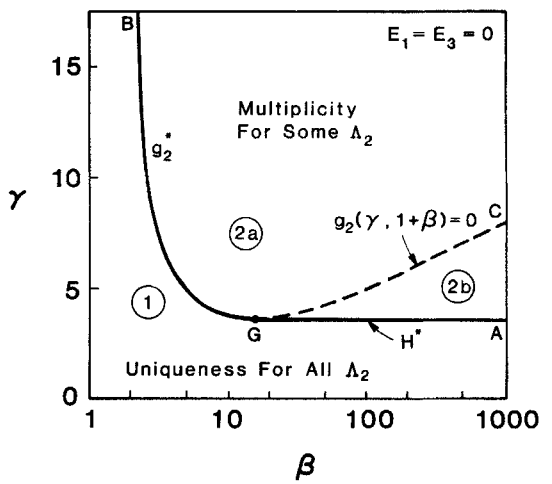

Figure 6. Uniqueness boundary g_2^* and H^* in (γ, β) plane for limiting case *b* (turbulent pressure loss).

set, while those for $\beta > 15.22$ (dashed line GC in Figure 6) do not satisfy that condition and are not members of the g_2^* set.

The g_2^* and H^* curves divide the (γ, β) plane into two regions in Figure 6. In region 1 Da is a monotonic increasing function of Π_1. In region 2 the bifurcation diagram of Da vs. Π_1 has an S shape. At the ignition point $Da < Da^*$, i.e., the reactant is not completely consumed. The solutions of $g_2(\gamma, 1 + \beta) = 0$ that do not satisfy condition Eq. 36c divide this region into two parts. For parameters in region 2a the conversion is complete at the extinction point ($Da > Da^*$), while in region 2b the reactant is not completely consumed at the extinction point. Note that $\beta > 15.22$ in region 2b and such high values are not encountered in practice.

The points on g_2^* that satisfy steady state Eq. 47 for some feasible Λ_2 are members of the GH variety. To find these points we combine Eqs. 25 and 47 to get

$$\frac{1}{\Lambda_2 \beta^2} = \frac{2J(y_1, 1)}{J^3(y_1, 0)}. \tag{52}$$

Solving Eq. 52 for $y_1 = 1 + \beta$ for (γ, β) values on g_2^* we find that the value of Λ_2 at the hysteresis point increases from 4.44×10^{-4} at point G to 1.88×10^{-3} at $\gamma^* = 5.333$ and $\beta^* = 4.278$. The value of Λ_2 decreases monotonically to zero for β values to the left of β^*. On the H^* curve $\Lambda_2 \beta^2 = 0.103$, and the value of Λ_2 decreases monotonically from 4.44×10^{-4} at G to zero at $\beta = \infty$ (point A). These results imply that a hysteresis point cannot exist in the feasible region if

$$\Lambda_{2\ell} = \frac{E_2}{1 - \Pi_\ell^2} > 1.88 \times 10^{-3}. \tag{53}$$

This is a sufficient uniqueness criterion for all (γ, β) values. The shapes of the g_2^* and H^* curves shown in Figure 6 imply that uniqueness is guaranteed for all feasible exit pressures if either

$$\gamma < 3.65 \tag{54}$$

or

$$\beta < 2. \tag{55}$$

Steady state multiplicity can be observed only if the exit pressure at the ignition point exceeds the limiting value ($\Pi_1 > \Pi_\ell$). For any $\Lambda_{2\ell} < 1.88 \times 10^{-3}$, the multiplicity region is bounded between the feasible part of the AB curve, Figure 6, and a BLS_1. This set can be constructed by a simultaneous solution of Eqs. 50 and 52 for the specific $\Lambda_{2\ell}$ using y_1 as a parameter. A simultaneous solution of these two equations gives the curve shown in Figure 7. Steady state multiplicity can be found (ignition point is within the feasible region) only for parameters in the hatched area in that figure, which indicates that multiplicity cannot occur if

$$\beta^2 \Lambda_{2\ell} > 0.103. \tag{56}$$

For any $\Lambda_{2\ell} < 1.88 \times 10^{-3}$, the multiplicity region is bounded by the g_2^* and H^* curves shown in Figure 6 and the BLS_1 curve shown in Figure 7. For $\Lambda_{2\ell}$ in $(4.44 \times 10^{-4}, 1.88 \times 10^{-3})$ the

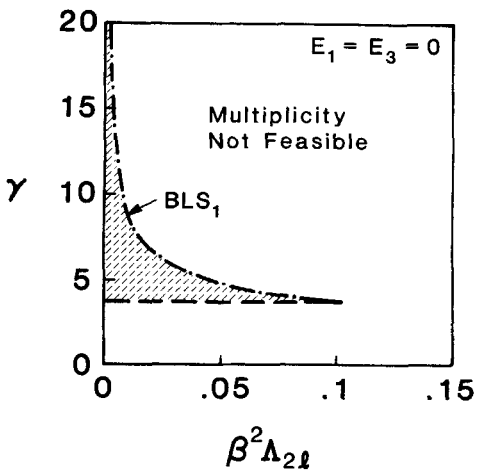

Figure 7. Dependence of uniqueness boundary BLS_1 on γ and $\beta^2\Lambda_{2\ell}$ for limiting case *b* (turbulent pressure loss).

BLS_1 intersects the g_2^* curve twice while for $\Lambda_{2\ell}$ in $(0, 4.44 \times 10^{-4})$ it intersects the g_2^* curve once and the H^* curve once. A typical case is illustrated in Figure 8. The BLS_2 is the boundary at which the extinction shifts from above to below the limiting pressure. It is found by a simultaneous solution of either Eq. 48 and $dF_2/dDa = 0$ in region *2a* in Figure 6 or Eqs. 50 and 52 in region *2b*.

The hysteresis, generalized hysteresis, and boundary limit sets divide the (γ, β) plane into three regions corresponding to the three types of bifurcation diagrams shown in Figure 1.

The above analysis indicates that thermoflow multiplicity cannot occur if any one of condition Eqs. 53–56 is satisfied. Multiplicity occurs for some Π_1 only if all these four conditions are violated. These conditions are more restrictive than those obtained in case *a*, indicating that this limiting model is less likely to predict multiplicity.

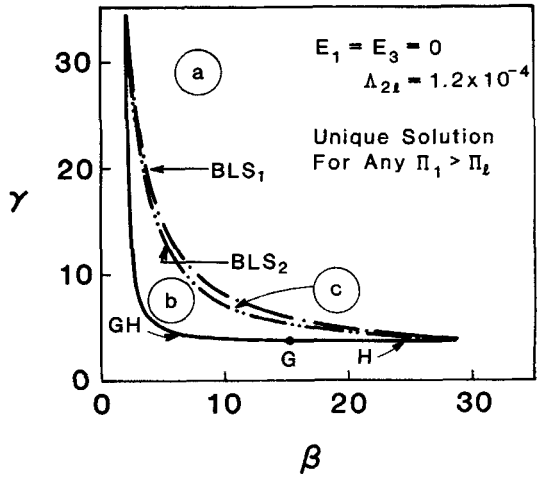

Figure 8. Division of (γ, β) plane into regions with different Da vs. Π_1 bifurcation diagrams for limiting case b.

Letters refer to diagrams shown in Figure 1.

Limiting case c, momentum change by gas expansion

This limiting case of $E_1 = E_2 = 0$ describes a situation in which the frictional pressure drop is negligible in comparison to the momentum change generated by the thermal expansion of the reacting fluid. This qualitatively different feedback mechanism leads to some novel features not found in the first two limiting cases.

Steady state Eqs. 33 and 34 simplify in this case to

$$F_1(Da, \Lambda_3, p) = \frac{1}{\Lambda_3} - \frac{2(y_1 - 1)}{Da^2} = 0 \tag{57}$$

where y_1 satisfies Eq. 25 and

$$F_2(Da, \Lambda_3, p) = \frac{1}{\Lambda_3} - \frac{2\beta}{Da^2} = 0. \tag{58}$$

Inspection of Eq. 58 indicates that dF_2/dDa is always positive so that no regular limit point or hysteresis variety exists for any $Da > Da^*$. Equations 35b and 35c with $i = 1$ have for all $\beta > 2.838$ the solution

$$\gamma = 2.596 \quad y_1 = 3.838. \tag{59}$$

Thus, the H^* set (solid line segment GA in Figure 9) consists of the line $\gamma = 2.596$ for $\beta > 2.838$.

To construct the GH, we first use Eqs. 25 and 57 to show that the condition $dF_1/dDa = 0$ is equivalent to

$$g_3(\gamma, y_1) = 2(y_1 - 1) - X(y_1)J(y_1, 0) = 0. \tag{60}$$

A unique γ value satisfies the equation

$$g_3(\gamma, 1 + \beta) = \beta\left\{2 - \int_o^1 \exp\left[\frac{\gamma\beta(1-u)}{(1+\beta)(1+\beta u)}\right]du\right\} = 0 \tag{61}$$

for any positive β. For sufficiently small β the solutions of Eq. 61 approach asymptotically (from above) the curve $\exp(\gamma\beta) = 1 + 2(\gamma\beta)$, or equivalently $\gamma\beta = 1.256$. In fact, Eq. 61 has no solution for

$$\gamma\beta < 1.256. \tag{62}$$

The solutions of Eq. 61 with $\beta < 2.838$ (solid line segment GB in Figure 9) satisfy condition Eq. 36c and belong to the g_3^* set. The solutions for $\beta > 2.838$ (dashed line GC in Figure 9) do not satisfy Eq. 36c and are not members of the g_3^* set.

The H^* and g_3^* curves divide the (γ, β) plane in Figure 9 into two regions. In region *1* Da is a monotonic increasing function of Π_1, while in region *2* the bifurcation diagram has an S shape with an ignition point at $Da < Da^*$. The $g_3(\gamma, 1 + \beta) = 0$ curve divides region 2 into two subregions. In region 2b the extinction occurs for $Da < Da^*$. In region 2a the extinction point occurs at $Da = Da^*$ and is a generalized limit point satisfying the condition

$$F_1(Da^* - \epsilon)F_2(Da^* + \epsilon) > 0 \tag{63}$$

where ϵ is an arbitrarily small positive number. Points on the g_3^* curve that satisfy steady state Eq. 57 for some feasible Λ_3 are

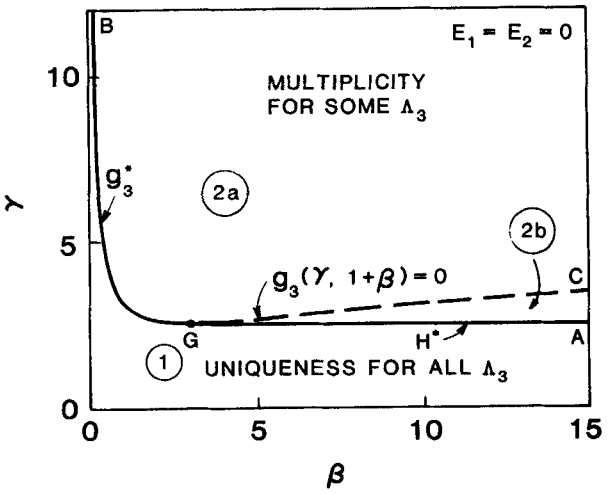

Figure 9. Uniqueness boundaries g_3^* and H^* in (γ, β) plane for limiting case *c* (gas expansion).

members of the GH variety. To find the values of Λ_3 for which a generalized cusp point exists we combine Eqs. 25 and 57 to get

$$\frac{1}{\Lambda_3\beta^2} = \frac{2(y_1 - 1)}{J^2(y_1, 0)}. \tag{64}$$

Solving Eqs. 64 for $y_1 = 1 + \beta$ and (γ, β) values on g_3^*, we find that the value of Λ_3 at the hysteresis point increases monotonically from 0.01515 (at point G) to infinity for $\beta \to 0$ (point B). Along the H^* curve GA, $\Lambda_3\beta^2 = 0.1222$ and Λ_3 decreases monotonically to zero for $\beta \to \infty$.

Points on BLS_1 are found by a simultaneous solution of Eqs. 60 and 64 for a specific $\Lambda_{3\ell}$ using y_1 as a parameter. Figure 10 describes the γ vs. $\beta^2\Lambda_3$ dependence obtained by a simultaneous solution of the two equations. Clearly, multiplicity can be found only for parameters to the left of this curve and for $\gamma > 2.596$. The figure shows that a sufficient uniqueness condition is

$$\beta^2\Lambda_{3\ell} > 0.1222 \tag{65}$$

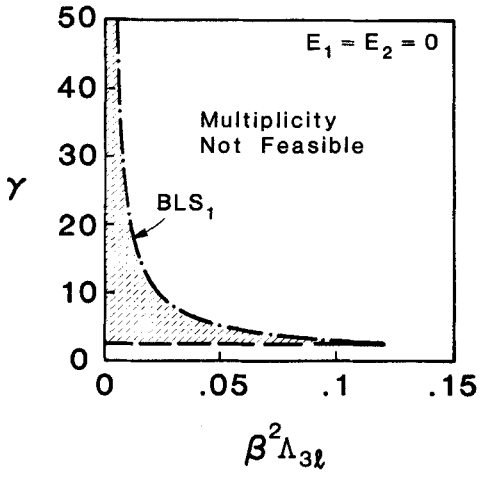

Figure 10. Dependence of uniqueness boundary BLS_1 on γ and $\beta^2\ \Lambda_{3\ell}$ for limiting case *c* (gas expansion).

The BLS_2 in region 2b of Figure 9 can be found by solving Eqs. 60 and 64 for a specific $\Lambda_{3\ell}$. In region 2a the extinction point is a generalized limit point and the BLS_2 is found by solving Eq. 64 with $y_1 = 1 + \beta$ for a specific $\Lambda_{3\ell}$.

In this limiting case, unlike the previous two, a multiplicity region exists in the (γ, β) plane for all positive $\Lambda_{3\ell}$ values. The size of this region increases with decreasing $\Lambda_{3\ell}$ values. For all $\Lambda_{3\ell}$ in (0, 0.01515) a cusp formed by the BLS_1 and BLS_2 emanates from the H set, Figure 11b, while for $\Lambda_{3\ell} > 0.01515$ the BLS_1 and BLS_2 emanate from the GH set, Figure 11a. The two branches of the BLS_1 and BLS_2 extend to unbounded γ values without intersecting the GH, i.e., the multiplicity region is not bounded.

The bifurcation diagrams of Da vs. Π_1 obtained in this limiting case are rather similar to those obtained in the first two limiting cases except for the discontinuity in the slope at $Da = Da^*$. Figure 12 shows two typical cases corresponding to the behavior in regions *1* and *2a* in Figure 9.

The analysis indicates that a unique solution exists whenever

$$\gamma < 2.596 \tag{66}$$

or if condition Eqs. 62 or 65 are satisfied. Multiple solutions can exist for some Π_1 only if all three conditions are violated. These conditions are less restrictive than those for case *b* and those for case *a* for β smaller than 1.50. It should be noted that for limiting case *c* multiple solutions can exist for arbitrarily small β in contrast to limiting cases *a* and *b*.

Steady state Eqs. 57 and 58 take a simpler form when the positive exponential approximation is used. Analytical solutions for

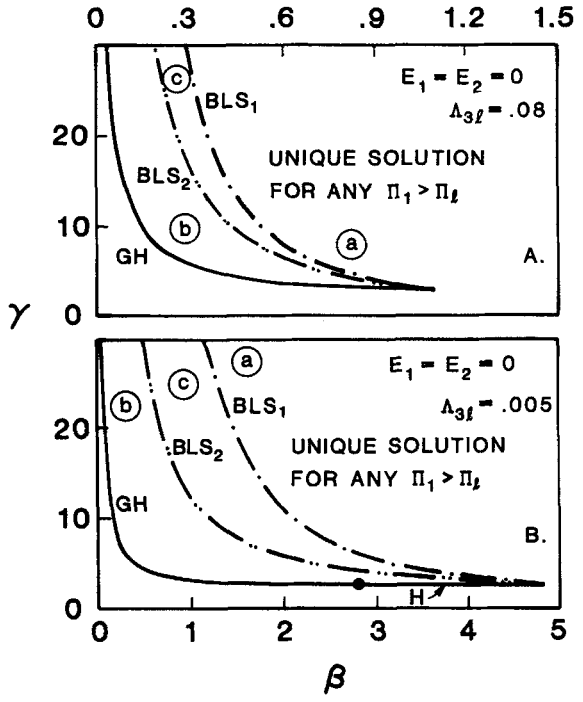

Figure 11. Division of (γ, β) plane into regions with different Da vs. Π_1 bifurcation diagrams for limiting case *c*.

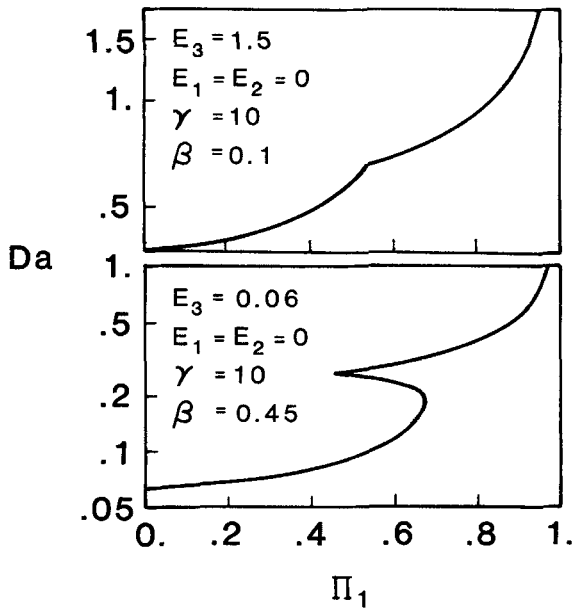

Figure 12. Two typical bifurcation diagrams for limiting case *c* (gas expansion).

the temperature, pressure and velocity profiles for this special case are given in the Appendix.

Limiting case d, $E_1 = 0$, turbulent pressure loss and gas expansion

This limiting case accounts for the two types of momentum changes considered separately in limiting models *b* and *c*, namely the turbulent frictional pressure drop and the thermal expansion of the gas. This limiting case ignores the laminar pressure drop described by the first term in the Ergun equation.

Steady state Eqs. 33 and 34 simplify in this case to

$$F_1 = \frac{1}{\Lambda_2} - \left[\frac{2J(y_1, 1)}{\beta Da^3} + \frac{2(y_1 - 1)E_3/E_2}{Da^2}\right] = 0 \tag{67}$$

$$F_2 = \frac{1}{\Lambda_2} - \left\{\frac{2J(1+\beta, 1)}{\beta Da^3} + \frac{2(1+\beta)}{Da^2} \cdot \left[1 - \frac{J(1+\beta, 0)}{\beta Da}\right] + \frac{2\beta E_3/E_2}{Da^2}\right\} = 0. \tag{68}$$

The behavior in this case was found to be rather similar to that of limiting cases *b* and *c*. Namely, no hysteresis variety exists for F_2. On the other hand a H^* set that satisfies Eqs. 35b and 35c exists for all $\beta > \bar{\beta}$ at

$$\gamma = \bar{\gamma} \quad y_1 = \bar{y} = 1 + \bar{\beta} \tag{69}$$

where $\bar{\beta}$, $\bar{\gamma}$, and $\bar{y}$ are monotonic decreasing functions of the ratio E_3/E_2. The value of $\bar{\gamma}(\bar{y})$ is 3.65 (16.22) for $E_3/E_2 = 0$ and 2.596 (3.838) for $E_3/E_2 = \infty$. Figure 13 describes H^* curves (dashed lines) for several E_3/E_2 values.

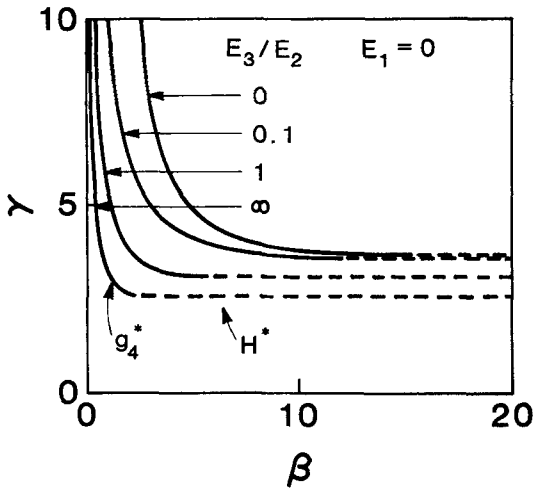

Figure 13. Dependence of uniqueness boundaries g_4^* and H^* on E_3/E_2 for limiting case *d* (turbulent pressure loss and gas expansion).

Condition Eq. 36b becomes in this case

$$g_4(\gamma, 1+\beta) \equiv E_2 g_2(\gamma, 1+\beta) + E_3 J(1+\beta, 0) g_3(\gamma, 1+\beta) = 0. \quad (70)$$

A unique value of γ satisfies Eq. 70 for any β. All the solutions for $\beta < \bar{\beta}$ satisfy Eq. 36c and are therefore members of the g_4^* set for the specific E_3/E_2 (solid lines in Figure 13). The calculations show that for any $E_3/E_2 > 0$ the g_4^* curve is bounded between g_2^* and g_3^* and approaches aymptotically $\beta = 0$ for sufficiently large γ. Clearly, the condition in Eq. 62 is sufficient for uniqueness.

Steady state multiplicity occurs for some (γ, β) values only if a GH exists, i.e., steady state Eq. 67 is satisfied for some points on the g_4^* curve. The Λ_2 values on any g_4^* curves with $E_3/E_2 > 0.013$ attain a unique maximal value, denoted by M_1 in Figure 14a. For any $E_3/E_2 < 0.013$ two local maximal values of Λ_2 (M_1 and M_2) and one minimal value of Λ_2 (denoted by m_1) exist on any g_4^* curve. These values are shown in Figure 14b.

A GH does not exist if Λ_{2g} exceeds M_1 for $E_3/E_2 > 0.013$ or both M_1 and M_2 for $E_3/E_2 < 0.013$. In such cases a unique solution exists for any feasible Λ_2 (exit pressure). Multiplicity exists for some Λ_2 and (γ, β) values in a crescent or wedge shaped region if Λ_{2g} is smaller than M_1 for $E_3/E_2 > 0.013$, and if Λ_{2g} is either bounded between M_1 and M_2 or smaller than m_1 for $E_3/E_2 < 0.013$.

The coupling between the two pressure loss mechanisms can create a novel qualitative feature, namely, two separated multiplicity regions in the (γ, β) plane. This can occur when $E_3/E_2 < 0.013$ and Λ_{2g} is smaller than both M_1 and M_2 but larger than m_1. One of these two multiplicity regions exists for β values to the left of (smaller than) m_1 and the other for β values to the right of m_1 in the (γ, β) plane. Numerical computations show that β is larger than 1.934 at m_1 for any E_3/E_2. Thus, one of these two regions occurs for unrealistically high β values (>1.934) and is not observable in practice. The calculations show that the two separated multiplicity regions are very narrow. Under most practical conditions one region of multiplicity exists as in the previous limiting models.

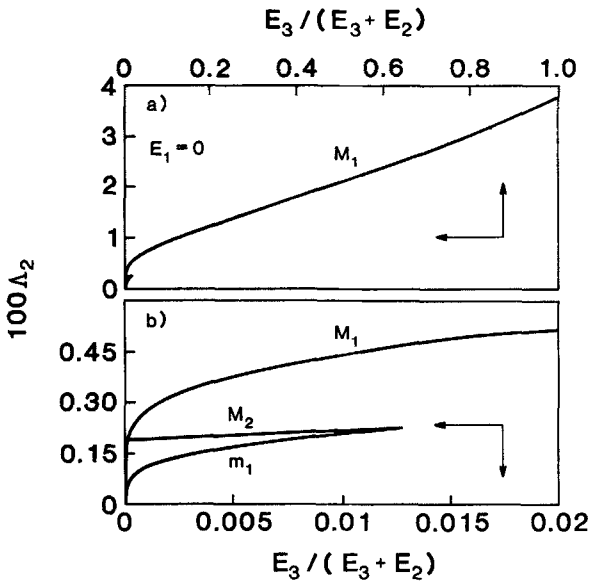

Figure 14. Dependence of maximum (M_1 and M_2) and minimum values of Λ_2 at the hysteresis point on $E_3/(E_2 + E_3)$.

The BLS_1 is determined by the simultaneous solution of $F_1 = dF_1/dDa = 0$ for $\Lambda_2 = \Lambda_{2g}$. It is possible to plot a graph of the BLS_1 for any specific E_3/E_2 in the $(\gamma, \beta^2\Lambda_{2g})$ plane (as was done in Figure 8 for limiting case *b*) or in the $(\gamma, \beta^2\Lambda_{3g})$ plane (as was done in Figure 10 for limiting case *c*). Along these curves $\gamma \to \infty$ as $\beta \to 0$ and γ decreases monotonically with increasing $\beta^2\Lambda_{ig}$ ($i = 2$ or 3). The smallest feasible γ value corresponds to H^*. Numerical calculations showed that $\beta^2\Lambda_{2g}(\beta^2\Lambda_{3g})$ at H^* decreases (increases) with E_3/E_2. These curves can be used to check if multiplicity can occur. They show that multiplicity cannot exist for any E_3/E_2 if either $\beta^2\Lambda_{2g} > 1.03$ (the value at H^* for limiting case *b*) or if $\beta^2\Lambda_{3g} > 0.122$ (the value at H^* for limiting case *c*).

Figure 13 indicates that the g_4^* curves are shifted to the right in the γ-β plane with decreasing E_3/E_2. It can be proven that for the same γ that the value of Λ_3 at the ignition point (if one exists) decreases with decreasing E_3/E_2. Thus if for a fixed Λ_{3g} the ratio of E_3/E_2 is decreased, the g_4^* curve moves to the right in the (γ, β) plane, while the BLS_1 line moves to the left and the size of the multiplicity region is reduced. In fact, for a fixed Λ_{3g} the multiplicity region for any E_3/E_2 is completely bounded within that for larger E_3/E_2 values. We conclude that *if for a given Λ_{3g} a multiplicity region does not exist in case c ($E_1 = E_2 = 0$) then multiplicity does not exist for case d.* Thus, the sufficient uniqueness criteria for case *c* can be applied directly in this case.

Limiting case e, $E_2 = 0$, laminar pressure drop and gas expansion

This limiting case accounts for the two feedback mechanisms considered separately in limiting cases *a* and *c*, i.e., it assumes that the second term in the Ergun equation is negligible in comparison to the first. To minimize the number of the parameters we assume that $\delta = 0.5$.

Steady state Eqs. 33 and 34 simplify in this case to

$$F_1 = \frac{1}{\Lambda_1} - 2\left[\frac{J(y_1, 1.5)}{\beta Da^2} + \frac{(y_1 - 1)E_3/E_1}{Da^2}\right] = 0 \quad (71)$$

$$F_2 = \frac{1}{\Lambda_1} - 2\left\{\frac{J(1+\beta, 1.5)}{\beta Da^2} + \frac{(1+\beta)^{1.5}}{Da} \cdot \left[1 - \frac{J(1+\beta, 0)}{\beta Da}\right] + \frac{\beta E_3/E_1}{Da^2}\right\} = 0. \quad (72)$$

No hysteresis variety of F_2 exists in this case and a limit (extinction) point is the only singularity that exists for $Da > Da^*$. The function F is continuous for all Da but dF/dDa is discontinuous at Da^*. The interaction between the two momentum transport mechanisms leads to novel qualitative features not observed in any of the first four limiting cases. For example, a generalized butterfly point, which satisfies the following conditions

$$F_1 = \frac{dF_1}{dDa} = \frac{d^2F_1}{dDa^2} = \frac{d^3F_1}{dDa^3} = 0 \quad (73a)$$

and

$$F_1(Da^* - \epsilon)F_2(Da^* + \epsilon) < 0 \quad (73b)$$

exists at

$$\gamma = 2.43 \quad \beta = 5.91 \quad E_3/E_1 = 1.08.$$
$$\Lambda_1 = 3.25 \times 10^{-3} \quad Da^* = 0.224. \quad (74)$$

Moreover, there exists a family of swallowtail points satisfying Eq. 73a for $Da < Da^*$ as well as a family of generalized swallowtail points satisfying

$$F_1 = \frac{dF_1}{dDa} = \frac{d^2F_1}{dDa^2} = 0 \quad (75)$$

$$F_1(Da^* - \epsilon)F_2(Da^* + \epsilon) > 0 \quad (76)$$

at $Da = Da^*$. Thus, while at most three steady state solutions exist for any set of parameters in all the previous limiting cases, five solutions exist for some parameters in this case. This indicates that the interaction between cases *a* and *c* is qualitatively different from that between cases *b* and *c*.

The boundaries of the multiplicity region in the (γ, β) plane are found again by the construction of the H and GH varieties and the BLS_1. We shall not report here all the algebraic manipulations, for they can be found elsewhere (Lee, 1987).

We denote by g_5^* the set of (γ, β) values that satisfy Eqs. 36b and 36c and by H^* those that satisfy Eqs. 35b and 35c. Each of these sets is defined for a specific E_3/E_1 ratio.

Calculations show that the graph of g_5^* (solid lines in Figure 15) consists in general of two separated sections one of which is connected to the H^* graph (dashed lines). The graphs of g_5^* and H^* can have three different shapes depending on the values of E_3/E_1.

For $E_3/E_1 > 1.08$ one branch of the g_5^* emanates at a relatively large β value from the β axis (case *a* in Figure 15), while

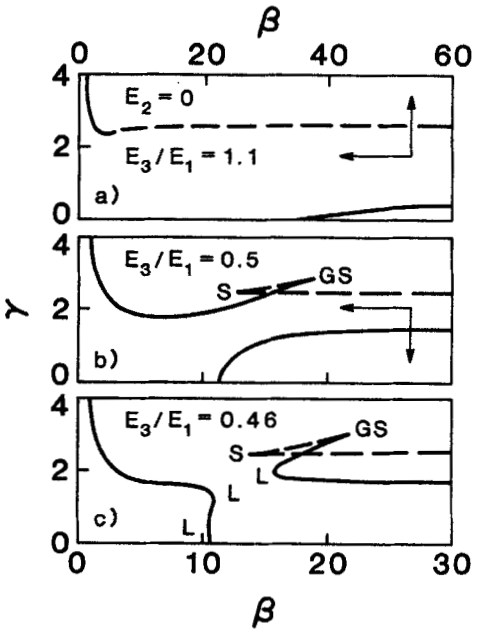

Figure 15. Three cross sections of the hysteresis (solid line) generalized hysteresis variety (dashed line) for limiting case *e* (laminar pressure loss and gas expansion).

the other branch of g_5^* and H^* form a continuous curve in the (γ, β) plane.

For any E_3/E_1 in (1.08, 0) the g_5^* and H^* branches form a pocket in the (γ, β) plane. We denote by *GS* the point formed by the tangential intersection of g_5^* and H^* and by *S* the point at which the two H^* branches meet. Point *GS* is a generalized swallowtail point if steady state Eq. 71 is satisfied at that point for $y_1 = 1 + \beta$ and some feasible Λ_1, while *S* is a swallowtail point if Eq. 71 is satisfied for some Λ_1. At *S*

$$\gamma = 2.43 \quad y_1 = 6.91 \quad \beta = 6.38\, E_1/E_3. \quad (77)$$

Clearly, *S* must be to the right of $\beta = 5.91$ and it is shifted to higher β as E_1/E_3 is increased. The swallowtail points *S* and *GS* coalesce at the generalized butterfly point defined by Eq. 74.

The two g_5^* branches touch and form an isola point at

$$E_3/E_1 = 0.468 \quad \beta = 12.68 \quad \gamma = 1.592 \quad (78)$$

For E_3/E_1 in (0.474, 1.08) the g_5^* and H^* branches have the shape shown in case *b* in Figure 15. For E_3/E_1 in (0.468, 0.474) a limit point *L* exists on the lower branch of g_5^* and it moves to higher γ values as E_3/E_1 is decreased. When $E_3/E_1 = 0.474$, this limit point is on the $\gamma = 0$ axis at $\beta = 10.666$.

For all E_3/E_1 in (0.4462, 0.468) these curves have the shape shown as case *c* and the g_5^* has three limit points, denoted by *L*. One is on the right branch of g_5^* and two are on the left branch. These two occur for rather close β values, and coalesce at $E_3/E_1 = 0.4462$ ($\gamma = 0.62$ $\beta = 9.889$). For all E_3/E_1 in (0, 0.4462) the shape of g_5^* is similar to that in case *c* but no limit point exists on the left branch.

The bifurcation diagram of *Da* vs. Π_1 has four limit points for all (γ, β) values within the pocket. The double limit variety divides the pocket into five regions corresponding to five dif-

ferent types of bifurcation diagrams. In four of these regions, five values of Da, or equivalently of u_o, exist for the same exit pressure Π_1. This pocket is always to the right of point S and thus exists only for unrealistically high values of β (>5.91). The model predicts that at most three solutions exist for realistic β values. Thus, we do not describe here the multiplicity regions found when the pocket exists and refer the interested reader to Lee (1987).

The existence of five solutions for all $0 < E_3/E_1 < 1.08$ indicates that the solution structure of this model for any arbitrarily small E_3 is different from that of limiting case a ($E_3 = 0$), for which at most three solutions exist. We refer to this feature as the *structural sensitivity* of limiting model a.

In practice β is always smaller than 2 and we examine therefore the shape of g_5^* in this feasible region, Figure 16. (H^* does not exist for $\beta < 2.838$ for any E_3/E_1). It can be shown that

$$g_5(\gamma, 1+\beta) \equiv E_1 g_1(\gamma, 1+\beta) + \beta E_3 g_3(\gamma, 1+\beta) = 0. \quad (79)$$

For any E_3/E_1 value, the graph of g_5^* passes through the point

$$\gamma = 2.76 \quad \beta = 1.50 \quad (80)$$

at which

$$g_1 = g_3 = 0. \quad (81)$$

For all $\beta < 1.50$ the g_5^* curves are bounded from below by g_3^* and from above by g_1^*. These bounds interchange their role in $1.5 < \beta < 2$, Figure 16. All the g_5^* curves for $E_3 > 0$ tend asymptotically to $\beta = 0$ for sufficiently large γ values.

Figure 17 shows a typical multiplicity region in the (γ, β) plane. The region extends to β values larger than 2, but this part of the region is not shown. It is noted that multiplicity can occur for very small β values if the activation energy is sufficiently large. Both the GH and BLS_1, intersect the $\gamma = 0$ axis for β values outside this graph. This indicates that multiplicity may occur for arbitrarily small activation energies.

It can be proven that *for any* (γ, β) *values bounded by* BO

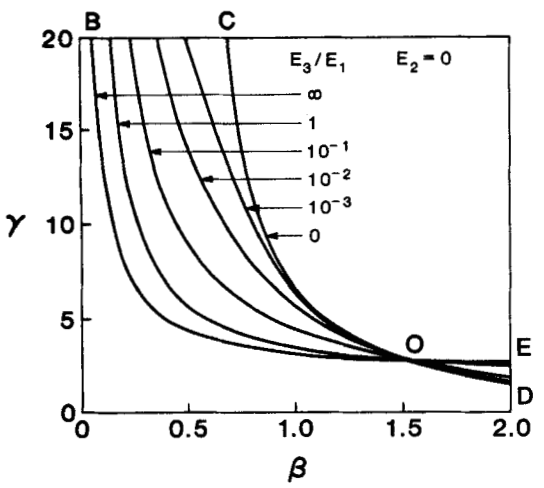

Figure 16. Dependence of uniqueness boundary g_5^* on E_3/E_1 for limiting case *e* (laminar pressure loss and gas expansion).

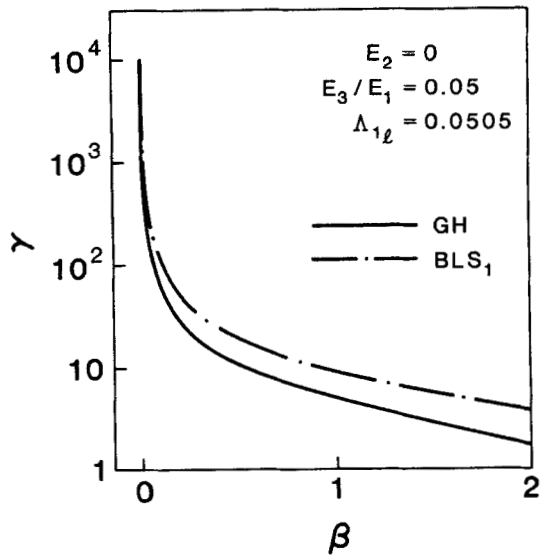

Figure 17. Region of multiplicity in (γ, β) plane for case *e*.

and OC *in Figure 16 multiplicity can occur for any* $\Lambda_{3\ell}$ *only if it occurs for case* c. *Similarly, for all* (γ, β) *bounded between the* g_5^* branches OD *and* OE *multiplicity can exist for some* $\Lambda_{1\ell}$ *only if it exists for case* a. *For all* (γ, β) *to the right of the* g_5^* branches OC *and* OE *multiplicity can occur only if it exists in limiting case* a *for the same* $\Lambda_{1\ell}$ *and in the limiting case* c *for the same* $\Lambda_{3\ell}$.

Limiting case f, $E_3 = 0$, laminar and turbulent pressure drop

This limiting case accounts only for the momentum change due to the frictional pressure loss and ignores the impact of the thermal expansion of the fluid on the momentum balance. Steady state Eqs. 33 and 34 reduce in this case to

$$F_1 = \frac{1}{\Lambda_1} - 2\left[\frac{J(y_1, 1.5)}{\beta Da^2} + \frac{J(y_1, 1)E_2/E_1}{\beta Da^3}\right] = 0 \quad (82)$$

$$F_2 = \frac{1}{\Lambda_1} - 2\left\{\frac{J(1+\beta, 1.5)}{\beta Da^2} + \frac{J(1+\beta, 1)E_2/E_1}{\beta Da^3} + \left[\frac{(1+\beta)^{1.5}}{Da} + \frac{(1+\beta)E_2/E_1}{Da^2}\right]\left[1 - \frac{J(1+\beta, 0)}{\beta Da}\right]\right\} = 0 \quad (83)$$

The behavior in this case is rather similar to that in case *e*. Again no hysteresis variety of F_2 exists and a limit (extinction) point is the singularity of the highest codimension that exists for $Da > Da^*$. The function F and dF/dDa are continuous for all Da but d^2F/dDa^2 is discontinuous at Da^*.

We denote by g_6^* the set of (γ, β) values that satisfy Eqs. 36b and 36c and by H^* those that satisfy Eqs. 35b and 35c. Each of these sets is defined for a fixed E_2/E_1 ratio. Figure 18 shows that there exist in this case three types of qualitatively different diagrams which are similar to those found in case *e* (Figure 15).

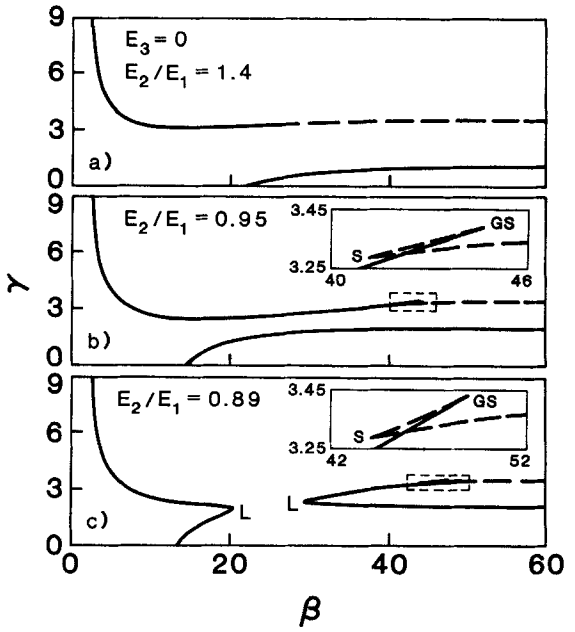

Figure 18. Three cross sections of the hysteresis (solid line) and generalized hysteresis variety (dashed line) for limiting case *f* (laminar and turbulent pressure loss).

For all $E_2/E_1 > 1.352$ (case *a* in Figure 18) the upper g_6^* branch is connected smoothly to the H^* branch, while the lower branch emanates from the β axis at large β values (>21.24). The g_6^* and H^* curves form a pocket for all E_2/E_1 in (0, 1.352). The *Da* vs. Π_1 diagram has four limit points for all (γ, β) values in the pocket. The point at which the g_6^* and H^* intersect tangentially is a generalized swallowtail point, denoted by *GS* in Figure 18, if it satisfies steady state Eq. 82 for some feasible Λ_1. The second corner, denoted by *S*, is a swallowtail point if Eq. 82 is satisfied for some Λ_1. At these *S* points

$$\gamma = 3.28 \quad y_1 = 29.86 \quad \beta = 39.03\, E_1/E_2. \tag{84}$$

Clearly, these points must be to the right of $\beta = 28.86$ and shift to higher β values with decreasing values of E_2/E_1.

The generalized and regular swallowtail points coalesce at

$$\gamma = 3.286 \quad \beta = 28.86 \quad E_2/E_1 = 1.352. \tag{85}$$

This point is a generalized butterfly point if steady state Eq. 82 is also satisfied there.

The two isolated branches of g_6^* touch each other as the parameters cross the isola point, located at

$$\gamma = 2.12 \quad \beta = 24.48 \quad E_2/E_1 = 0.90 \tag{86}$$

For all E_2/E_1 in (0.90, 1.352) the g_6^* and H^* have a shape similar to that of case *b* in Figure 18, while for all E_2/E_1 in (0, 0.90) they have the shape shown in case *c*.

The pocket of (γ, β) values for which four limit points exist is found for unrealistically high β values ($\beta > 28.86$) and at most three solutions exist for realistic β values. We note, however, that the limiting model *a* is structurally sensitive, as a qualitative change in its features (appearance of five solutions) may occur as we introduce an arbitrarily small value of E_2. We do not describe here the multiplicity features found when the pocket exists for very large β values, and refer the interested reader to Lee (1987).

Figure 19 describes the g_6^* curves for various E_2/E_1 ratios for β values smaller than 4. The calculations show that all the curves with a finite E_2/E_1 value approach asymptotically the g_2^* curve for large γ value, i.e., they approach $\beta = 2$. In fact, for all $E_2/E_1 > 0.533$ the g_6^* is to the right of $\beta = 2$ and a unique solution exists for any $\beta < 2$.

It can be proven (Lee, 1987) that Λ_1 at the ignition point for any finite E_2/E_1 is smaller, i.e., the exit pressure is smaller, than that at an ignition point for case *a* with the same (γ, β). Thus, *if multiplicity does not exist in case* a *for* $(\gamma, \beta, \Lambda_{1\ell})$ *then it cannot exist in case* f *for* $(\gamma, \beta, \Lambda_{1\ell})$ *and any* E_2/E_1. We conclude that all the sufficient uniqueness conditions for case *a* are still valid in case f.

Analysis of the General Case, E_1 E_2 $E_3 \neq 0$

The general case accounts for the two frictional pressure loss mechanisms and for the impact of the changes in the physical properties on the momentum balance. The steady state is described by Eqs. 33 and 34.

The qualitative features of the system are rather similar to those found for limiting cases *e* and *f*. No hysteresis variety of F_2 exists for any positive E_1, E_2, and E_3 values and a limit (extinction) point is the only singularity that may exist for any $Da > Da^*$.

The boundaries of regions with different types of bifurcation diagrams are found again by construction of the generalized and regular hysteresis variety, the double limit variety, and the BLS. The qualitative features of this case are similar to those of limiting cases *e* and *f* but the presentation is somewhat more intricate as the steady state equation contains an additional parameter. The singularity of the highest codimension is a generalized butterfly point, defined by Eqs. 73a, b. In fact, a line of generalized butterfly points exists, the projections of which onto the $E_3/$

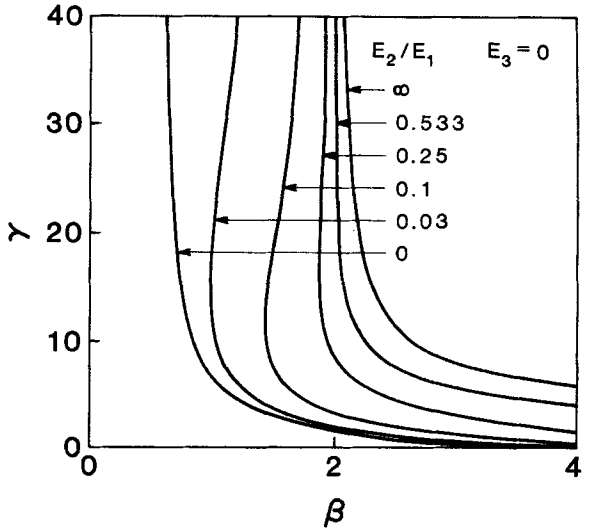

Figure 19. Dependence of uniqueness boundary g_6^* on E_2/E_1 for limiting case *f* (laminar and turbulent pressure loss).

$(E_1 + E_3)$, $E_2/(E_1 + E_2)$ plane is shown in Figure 20. This line divides this plane into two regions having qualitatively different g_7^* and H^* diagrams in the (γ, β) plane. For all $E_2/(E_1 + E_2)$ and $E_3/(E_1 + E_3)$ above or to the right of the line of generalized butterfly points the g_7^* graph is connected smoothly to the H^* graph and the shape of these two curves is similar to that in Figure 15a or 18a. The g_7^* branch that emanates from the β axis exists only for rather high β values (>21.24) and it is shifted to higher β values as E_3/E_1 and E_2/E_1 are increased. For all $E_2/(E_1 + E_2)$ and $E_3/(E_1 + E_3)$ values below or to the left of PQ, the line of the generalized butterfly points, the g_7^* and H^* form a pocket in the (γ, β) plane. Any bifurcation diagram of Da vs. Π_1 for any γ and β within the pocket has four limit points, and five solutions can be found for some γ and β values bounded within the pocket. This pocket exists only for unrealistically high β values (>5.91) and is not expected to be found under practical conditions. The relative position of the two g_7^* branches changes as $E_2/(E_1 + E_2)$ and $E_3/(E_1 + E_3)$ cross the isola variety of the function g_7^*. To the left of this variety the g_7^* and H^* curves have a shape similar to that shown in Figure 15c, while to the right of it their shape is similar to that shown in Figure 15b.

The four corner points A, B, C, and D correspond to the limiting cases a, b, c, and d, respectively, while the lines AC and AB correspond to limiting cases e and f. The diagram points out that the model for limiting case a (corner A) must be structurally sensitive as its maximal number of solutions for any $\Lambda_{1\ell}$ (three) is smaller than that obtained (five) for arbitrarily small values of E_2 and E_3 (points near corner A). This observation is mainly of theoretical significance, as for small E_1 and E_3 the pocket with the five solutions exists for unrealistically high β values.

The multiplicity features of this system are understood better by inspection of Figure 21, which describes the locus of the generalized butterfly points, line GH, and the surface of swallowtail points in the $[\Lambda_1, E_2/(E_1 + E_2), E_3/(E_1 + E_3)]$ space. Numerical calculations have shown that the largest Λ_1 value on the pocket of five solutions is at the swallowtail point. Thus, five solutions can exist only if $\Lambda_{1\ell}$ is smaller than the Λ_1 value at that point, which we denote as $\Lambda_1(S)$. We conclude that five solutions can be found only if $E_2/(E_1 + E_2)$, $E_3/(E_1 + E_3)$ are within the region OPQ in Figure 21, where PQ is the projection of the butterfly line HG onto the $\Lambda_1 = 0$ plane. In addition $\Lambda_{1\ell}$ must be below the surface of swallowtail points, OHG.

We shall not describe here the type of multiplicity regions and bifurcation diagrams that exist when β attains very high and unrealistic values and refer the interested reader to Lee (1987). Instead we describe here the behavior for $\beta < 2.5$.

The generalized hysteresis is found by constructing first the g_7^*curve, which is the set of (γ, β) values that satisfy for some Λ_1 Eqs. 36b and 36c for a specific set of E_2/E_1 and E_3/E_1. Equation 36b may be written

$$g_7(\gamma, 1 + \beta) \equiv E_1 J(1 + \beta, 0) g_1(\gamma, 1 + \beta) + E_2 \beta g_2(\gamma, 1 + \beta) + E_3 \beta J(1 + \beta, 0) g_3(\gamma, 1 + \beta) = 0. \quad (87)$$

The graph of g_i^* $(i = 1, 2, 3)$ is shown in Figure 22. Each of the g_i $(\gamma, 1 + \beta)$ is positive below the curve and negative above the curve. Thus, in region U all g_i are positive, and in region M all g_i are negative. We conclude that for any positive values of E_1, E_2, and E_3, the graph of Eq. 87 must be within the hatched area in Figure 22.

For (γ, β) values in region U in Figure 22, $d\Pi_1/dDa$ is positive for any Da and a unique solution exists for all (E_1, E_2, E_3) values. On the other hand, for (γ, β) values outside region U, there exist feasible values of (E_1, E_2, E_3) for which the bifurcation diagram of Da vs. Π_1 has two limit points, i.e., thermoflow multiplicity exists for some Π_1.

We conclude that knowledge of the g_i^* graphs for the first three limiting cases can be used to obtain sufficient uniqueness criteria and necessary multiplicity conditions for the general case. Thus, the criteria derived for these limiting cases are also useful in the general case.

Inspection of steady state Eqs. 33 and 34 indicates that for any γ, β, and Da the value of Λ_i ($i = 1$, 2, or 3) in the general case is smaller than the Λ_i in limiting case a, b, or c, respectively. In other words the graph of Da vs. Λ_i for the general case is bounded from below by that for any one of the three limiting cases. The value of Λ_i $(i = 1, 2, 3)$ at the ignition point for the

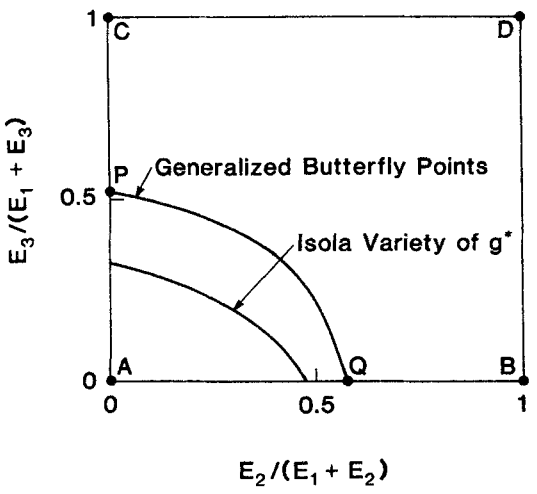

Figure 20. Projections of line of butterfly points and isola variety of g_7^* on $E_3/(E_1 + E_3)$ and $E_2/(E_1 + E_2)$ plane.

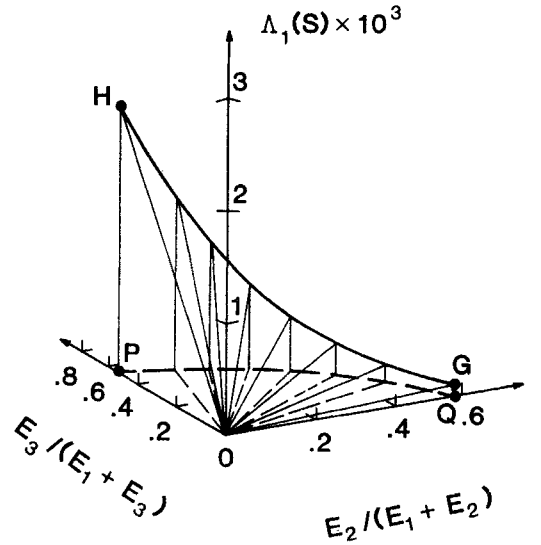

Figure 21. Locus of generalized butterfly points and surface of swallowtail points.

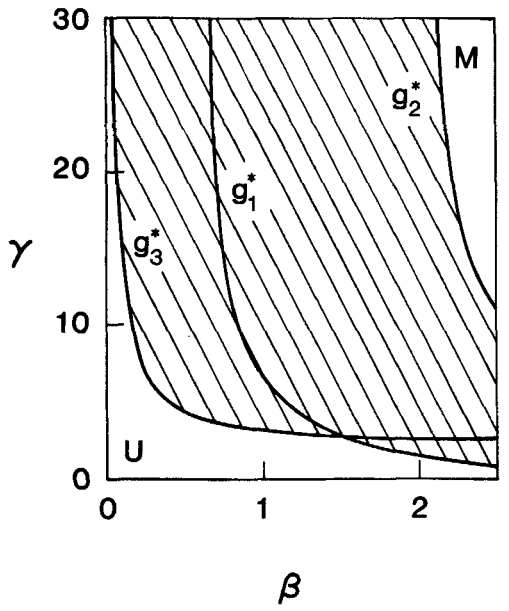

Figure 22. Graphs of g_i^* (i = 1, 2, 3) for $\beta < 2.5$.

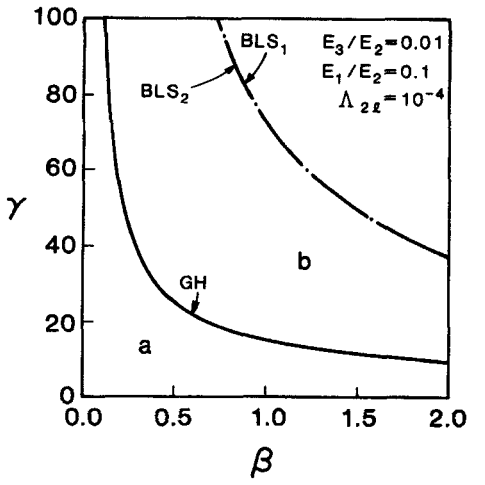

Figure 23. Division of (γ, β) plane into regions with qualitatively different *Da* vs. Π_1 bifurcation diagrams.
Letters refer to diagrams shown in Figure 1.

general case must be smaller than that for limiting case *a*, *b*, or *c*, respectively. Thus, multiplicity can be found only if $\Lambda_{i\ell}$ (i = 1, 2, 3) is smaller than that at the ignition point for limiting case *a*, *b*, or *c*, respectively. We conclude that uniqueness is guaranteed in the general case if one of the following three criteria is satisfied:

$$\Lambda_{1\ell} > 0.1032 \quad \text{when } (\gamma, \beta) \text{ is to the right of } g_1^* \tag{88}$$

$$\Lambda_{2\ell} > 1.88 \times 10^{-3} \quad \text{when } (\gamma, \beta) \text{ is to the right of } g_2^* \tag{89}$$

$$\Lambda_{3\ell}\beta^2 > 0.1222 \quad \text{when } (\gamma, \beta) \text{ is to the right of } g_3^*. \tag{90}$$

The exact location of g_i^* depends on the specific E_3/E_1 and E_2/E_1 values. The multiplicity region in the (γ, β) plane is bounded by the GH and the BLS$_1$ curves. For $\beta < 2.5$, there exists usually one such crescent-shaped region. However, for certain E_2/E_1 and E_3/E_1 there exists a range of $\Lambda_{i\ell}$ values for which two distinct, separated multiplicity regions exist. This may occur when the value of Λ_1 along g_1^* attains a local minimum within the feasible range of β values.

A typical hysteresis, BLS$_1$, and BLS$_2$ set is shown in Figure 23 for a set of parameters in region *CDBP* in Figure 20, i.e. in a region where at most three solutions exist. The BLS$_1$ and BLS$_2$ are very close to each other in this example and are therefore shown by the same curve in the figure. This figure indicates that three solutions can be found in the general case for realistic β values. It should be noted that one needs to construct the bifurcation diagram of *Da* vs. Π_1 to determine the range of pressures for which this multiplicity occurs for certain (γ, β) values.

It is of interest to check if this type of multiplicity may occur under practical conditions. Table 1 reports the values of the dimensionless parameters (γ, β, E_1, E_2, and E_3) for three industrial exothermic reactions. The (γ, β) values for these reactions are within the region in which multiplicity may occur. However, inspection indicates that the high values of E_1 and E_2 for napthalene oxidation imply that thermoflow multiplicity does not occur for that reaction.

The bottom row in the table describes the range of values these parameters may attain. It is noted that E_i may vary over a very wide range of conditions. The calculations show that in general E_2 is much larger than E_3. Inspection of Table 1 indicates that thermoflow multiplicity may occur for a realistic set of parameters.

The simulations have shown that for β values smaller than 2 the hysteresis loop is rather small. For example, when γ = 40, β = 1, $E_2 = 5 \times 10^{-5}$, $E_1 = 0.1\ E_2$, $E_3 = 0.01\ E_2$, multiplicity occurs when the dimensionless exit pressure is in the small range of (0.92204, 0.92257). The multiplicity occurs for a significantly larger range of exit pressures if $\beta > 2$.

The range of pressures for which multiplicity occurs can be expanded by modification of the model is discussed in the conclusions section.

Impact of the Assumption $\rho_o u_o^2 \ll P_o$

The analysis was carried out assuming that

$$\rho_o u_o^2 \ll P_o. \tag{91}$$

When this assumption is not made, Eq. 22 is of the form

$$\frac{1}{2}\left(1 - \frac{E_3 y}{Da^2\,\Pi^2}\right)\frac{d\Pi^2}{dz} = -\frac{E_1}{Da}y^{1+\delta} - \frac{E_2 y}{Da^2} - \frac{E_3}{Da^2}\frac{dy}{dz}. \tag{92}$$

To examine the impact of neglecting the second term in the

Table 1. Typical Values of the Dimensionless Parameters

Reaction	γ	β	E_1	E_2	E_3
Ethylene oxidation	10	1.3	10^{-5}	10^{-3}	10^{-7}
Methanol oxidation	10	0.8	10^{-6}	10^{-7}	10^{-9}
Napthalene oxidation	30	1.2	2.0	4.0	10^{-4}
Typical exothermic reaction	0–60	0–1.5	10^{-10}–10^{2}	10^{-10}–10^{3}	10^{-12}–10^{-2}

parentheses on the lefthand side of Eq. 92, we consider a case in which no chemical reaction occurs, i.e., $y = 1$. Integration of Eq. 92 gives

$$\frac{1}{2}(1 - \Pi_1^2)Da^2 - E_1 Da + E_3 \ln(\Pi_1) - E_2 = 0 \quad (93)$$

or equivalently

$$Da = \frac{E_1 + \sqrt{E_1^2 + 2(1 - \Pi_1^2)E_2[1 - E_3 \ln(\Pi_1)/E_2]}}{1 - \Pi_1^2} \quad (94)$$

Inspection of Eqs. 92 and 94 indicates that the assumption in Eq. 91 is equivalent to setting $E_3 = 0$ in Eq. 94.

Equation 94 predicts that for all positive E_3 Da becomes unbounded and $dDa/d\Pi_1$ is negative as $\Pi_1 \rightarrow 0$. By differentiation of Eq. 93 we find that $dDa/d\Pi_1$ vanishes when

$$E_1 + \sqrt{E_1^2 + 2(1 - \Pi_1^2)(E_2 - E_3 \ln \Pi_1)} = \frac{(1 - \Pi_1^2)\sqrt{E_3}}{\Pi_1} \quad (95)$$

For most practical cases $E_3/E_2 < 0.01$ and $E_1 < E_2$, and an approximate location of the minimum is given by

$$\Pi_1 \approx \frac{\sqrt{E_3}}{E_1 + \sqrt{E_1^2 + 2E_2}} \quad (96)$$

For practical values of E_i this value of Π_1 is much less than 0.1. Thus, the assumption in Eq. 91 affects the graph of Da vs. Π_1 only in a narrow region of very low exit pressures ($\Pi_1 < 0.1$). In practice, $\Pi_{1\ell}$ is usually larger than 0.5 and the term $E_3 \ln(\Pi_1)/E_2$ is very small compared to unity, so that neglecting it has a minor impact. The same is expected to hold when a chemical reaction occurs.

Conclusions and Remarks

This work shows that the coupling between the dependence of the heat generation on the feed flow rate and the change in the physical properties of the reacting stream may lead to thermoflow multiplicity in a packed-bed reactor operating under a fixed pressure drop. The mechanism of this multiplicity is conceptually different from that which has been considered traditionally in the reaction engineering literature, and it may occur even for reactions with very low activation energies, i.e., when the rate constant is rather insensitive to changes in the temperature.

Thermoflow multiplicity may lead to the existence of different temperature profiles in different tubes in a multitube reactor. This can have a deleterious effect on the yield of the desired product and lead to differences in the rate of deactivation of the catalyst in various tubes. Moreover, it may cause undesirable mechanical stresses that can damage the reactor.

The analysis points out that simplified models that do not account for the change of physical properties with temperature or conversion may yield erroneous qualitative predictions. Thus, it is essential to use a more detailed model, even though its analysis is more difficult. It is our belief that the coupling among the momentum, energy, and species balances and the change of physical properties is responsible for many effects that cannot be explained by models which account only for species and energy balances.

The analysis reveals that the criteria derived for each of the three limiting cases give simple criteria for the more general cases. This is a very useful result as it gives some simple practical guidance about the conditions that may lead to multiplicity.

The model used in this work is the simplest one that can account for thermoflow multiplicity. When the reaction involves an increase in the number of moles, the feedback is stronger and multiplicity can be observed over a wider range of parameters. An analysis of this effect will be presented elsewhere.

This work is restricted to the adiabatic case. This has the advantage of reducing the number of parameters in the model. In practice multitube reactors are being cooled. An analysis of the impact of the cooling will be presented elsewhere.

It is important to remember that the analysis and criteria presented here are for a zero-order reaction. The main advantage of analyzing the zero-order reaction is the ability to derive simple analytical multiplicity criteria and the ability to predict readily the structure of the solutions. We do not expect the use of other monotonic rate expressions to change the structure of the solutions and the multiplicity. However, this change may shift the region of the parameters for which multiplicity exists.

The model used in this work does not account for the transport resistances between the fluid and the catalyst or for the axial conductivity of heat. These two effects are the major causes of multiplicity in a reactor operating at a prescribed inlet velocity. The addition of these effects is certain to complicate the analysis but will probably expand significantly the range of parameters over which multiplicity will be observed for operation under a prescribed pressure drop.

We wish to point out that the analysis here is of gaseous reactions for which the viscosity increases with increasing temperature. For this case thermoflow multiplicity is found only for exothermic reactions, i.e., $\beta > 0$. However, as will be shown in more detail elsewhere, when the feed is incompressible and the viscosity decreases with increasing temperature, thermoflow multiplicity can be found only for endothermic reactions. This underscores very clearly the difference between the multiplicity caused by the thermoflow and thermokinetic mechanisms.

Acknowledgment

We are grateful to the American Chemical Society PRF and the National Science Foundation for support of this research.

Notation

A = constant in frictional pressure drop expression
B = constant in frictional pressure drop expression
C = concentration
c_p = heat capacity
Da = Damhkoler number, Eq. 20
Da^* = smallest Da for which conversion is complete
E = activation energy
E_1, E_2, E_3 = dimensionless parameters in momentum balance, Eq. 20
F = function defining steady state
F_1 = function defining steady state for $Da < Da^*$
F_2 = function defining steady state for $Da > Da^*$
f_p = frictional pressure drop gradient, Eq. 5
g^* = parameter set satisfying Eqs. 36b and 36c
H = Heaviside function
H^* = parameter set satisfying Eq. 35b and 35c
ΔH = heat of reaction
J = function, Eq. 26
$k(T)$ = reaction rate constant

L = length of reactor
ℓ = reactor length coordinate
M_W = molecular weight
P = pressure
p = parameter vector, Eq. 24
R = universal gas constant
r = reaction rate
T = temperature
u = velocity
X = function, Eq. 9
x = conversion
y = dimensionless temperature, Eq. 17
z = dimensionless reactor length coordinate, Eq. 20
z_c = position at which conversion is complete

Greek letters

β = adiabatic temperature rise, Eq. 17
Γ = function, Eq. 42
γ = dimensionless activation energy, Eq. 20
δ = constant, Eq. 9
Λ_j = parameter, Eq. 32, $j = 1, 2, 3$
μ = viscosity
Π = dimensionless pressure, Eq. 20
ρ = density

Subscripts

ℓ = limiting
O = inlet to reactor

Appendix

In limiting case c ($E_1 = E_2 = 0$) the energy and momentum balances can be written as

$$\frac{d\theta}{dz} = BDaX(\theta)H(B - \theta) \tag{A1}$$

$$\frac{1}{2}\frac{d\Pi^2}{dz} = -\frac{E_3}{\gamma Da^2}\frac{d\theta}{dz} \tag{A2}$$

where

$$\theta = \gamma(y - 1), \quad B = \gamma\beta. \tag{A3}$$

The positive exponential approximation is

$$X(\theta) = \frac{k(T)}{k(T_o)} = \exp(\theta). \tag{A4}$$

Integration of Eqs. A1 and A2 subject to the initial conditions

$$\theta = 0, \quad \Pi = 1 \quad \text{at } z = 0 \tag{A5}$$

gives the following analytical expressions for the temperature and pressure profiles

$$\theta(z) = \ln\left(\frac{1}{1 - BDaz}\right); \quad Da < Da^* \tag{A6}$$

$$\theta(z) = \begin{cases} \ln\left(\dfrac{1}{1 - BDaz}\right) & 0 < z < \dfrac{Da}{Da^*} \\ B, & \dfrac{Da}{Da^*} < z < 1 \end{cases}; \quad Da > Da^* \tag{A7}$$

$$\Pi(z) = \left[1 - \frac{2E_3}{\gamma Da^2}\theta(z)\right]^{0.5} \tag{A8}$$

where

$$Da^* = \frac{1 - \bar{e}^B}{B}. \tag{A9}$$

Defining

$$\lambda = \frac{\gamma[1 - \Pi(1)^2]}{2E_3} \tag{A10}$$

and combining Eqs. A6–A8 at $z = 1$ gives the following steady state equation:

$$f(Da, \lambda, B) \equiv \begin{cases} \dfrac{1}{Da^2}\ln\left(\dfrac{1}{1 - BDa}\right) - \lambda = 0; & Da < Da^* \\ \dfrac{B}{Da^2} - \lambda = 0; & Da > Da^* \end{cases} \tag{A11}$$

Equation A11 has a unique generalized hysteresis point at

$$Da^o = 0.569$$
$$\lambda^o = 3.876$$
$$B^o = 1.256. \tag{A12}$$

For $B < B^o$, the bifurcation diagram of Da vs. λ is single-valued. For $B > B^o$, the bifurcation diagram is S-shaped with an ignition point at

$$Da_i = \frac{0.715}{B}, \quad \lambda_i = 2.46B^2 \tag{A13}$$

and an extinction point at

$$Da_e = Da, \quad \lambda_e = \frac{B^3}{(1 - e^{-B})^2} \tag{A14}$$

Note that when multiplicity exists, two of the profiles are given by Eq. A6 and the third by Eq. A7.

Literature cited

Balakotaiah, V., and D. Luss, "Analysis of the Multiplicity Patterns of a CSTR," *Chem. Eng. Commun.*, **11**, 111 (1981).

———, "Global Analysis of the Multiplicity Features of Multireaction Lumped-Parameter Systems," *Chem. Eng. Sci.*, **39**, 865 (1984).

Bostandzhiyan, S. A., V. I. Boyarchenko, P. R. Zhirkov, and Zh. A. Zienko, "Low-Temperature Polymerization Conditions in a Flow-Through Reactor," *J. Appl. Mech. Tech. Phys.*, **20**(1), 99 (1979).

Davis, S. H., G. A. Kriegsmann, R. L. Laurence, and S. Rosenblat, "Multiple Solutions and Hysteresis in Steady Parallel Viscous Flows," *Phys. Fluids*, **26**, 1177 (1983).

Dogan, T., S. Kakac, and T. N. Veziroglu, "Analysis of Forced-Convection Boiling Flow Instabilities in a Single-Channel Upflow System," *Int. J. Heat Fluid Flow*, **4**, 145 (1983).

Goldshtik, M. A., "Thermochemical Instability of a Heat-Releasing Granular Layer," *12v. Akad. Nauk SSSR, Mekh. Zhidk Gaza*, No. 2, 45 (1979).

Gupalo, Yu. P., and S. Ryazantsev, "Thermochemical Instability in Steady Operating Regime of Continuous-Flow Chemical Reactor with Fixed Catalyzer Bed," *12v, Akad. Nauk SSSR, Mekh Zhidk. Gaza*, 3(2), 64 (1968).

Hegedus, L. L., S. H. Oh, and K. Baron, "Multiple Steady States in an Isothermal Integral Reactor; The Catalytic Oxidation of Carbon Monoxide over Platinum-Alumina," *AIChE J.*, **23**, 632 (1977).

Hlavacek, V., and J. Votruba, "Hysteresis and Periodic Activity Behavior in Catalytic Chemical Reaction Systems," *Adv. in Catal.*, **27**, 59 (1978).

Ledinegg, M., "Instability of Flow During Natural and Forced Convection," *Die Warme*, **61**, 891 (1938).

Lee, J. P., Ph.D. Thesis, "Thermoflow Multiplicity in a Packed-Bed Reactor," Univ. Houston, University Park, TX (1987).

Matros, Yu. Sh., and N. A. Chumakova, "Multiplicity of Stationary Regimes in an Adiabatic Catalyst Layer," *Dokl Akad Nauk SSSR*, **250**(6), 1421 (1980).

Merzhanov, A. G., and A. M. Stolin, "Hydrodynamic Analogies of the Phenomena of Ignition and Extinction," *J. Appl. Mech. Tech. Phys*, **15**(1), 53 (1974).

Paspek, S. C., and A. Varma, "An Experimental and Theoretical Investigation of Ethylene Oxidation on Supported Platinum in an Adiabatic Fixed-Bed Reactor," *Chem. Eng. Sci.*, **35**, 33 (1980).

Pearson, J. R. A., Y. T. Shah, and E. S. A. Vieira, "Stability of Nonisothermal Flow in Channels. I: Temperature-Dependent Newtonian Fluid without Heat Generation," *Chem. Eng. Sci.*, **28**, 2079 (1973).

Pearson, J. R. A., *Mechanics of Polymer Processing*, Elsevier, London (1985).

Sharma, C. S., and R. Hughes, "The Behavior of an Adiabatic Fixed-Bed Reactor for the Oxidation of Carbon Monoxide-2," *Chem. Eng. Sci.*, **34**, 625 (1979).

Vaganov, D. A., and P. V. Zhirkov, "Wavelike Transitions and Stability in Variable Viscosity Flows," *Chem. Eng. Sci.*, **41**, 237 (1986).

Wedel, S., and D. Luss, "Steady State Multiplicity Features of an Adiabatic Fixed-Bed Reactor with Langmuir-Hinshelwood Kinetics; CO or CO_2 Methanation," *Ind. Eng. Chem. Fundam.*, **23**, 280 (1984).

Zhirkov, P. V., S. A. Bostandzhiyan, and V. I. Boyarchenko, "Effect of Lengthwise Heat Transfer on the Process of Radical Polymerization in a Displacement Reactor," *J. Theor. Chem. Tech.*, **14**, 449 (1980).

Manuscript received Aug. 22, 1986, and revision received Oct. 2, 1986.